

23 **Abstract**

24 One of the most challenging tasks when studying large submarine landslides is determining
25 whether the landslide was initiated as a single large event, a chain of events closely spaced in
26 time or multiple events separated by long periods of time as all have implications in risk
27 assessments. In this study we combine new multichannel seismic profiles and new sediment
28 cores with bathymetric data to test whether the Rockall Bank Slide Complex, offshore western
29 Ireland, is the composite of multiple slope collapse events and, if so, to differentiate them. We
30 conclude that there have been at least three voluminous episodes of slope collapse separated by
31 long periods of slope stability, a fourth, less voluminous event, and possibly a fifth more
32 localized event. The oldest event, Slide A (200km³), is estimated to be several hundred thousand
33 years old. The second event, Slide B (125km³), took place at the same location as slide A,
34 reactivating the same scar, nearly 200 ka ago, possibly through retrogression of the scarp. Slide
35 C (400km³) took place 22 ka ago and occurred further north from the other slides. Slide D was a
36 much smaller event that happened 10 ka ago, while the most recent event, albeit very small-
37 scale, took place within the last 1000 years. This study highlights the need to thoroughly
38 investigate large slide complexes to evaluate event sequencing, as seismic studies may hide
39 multiple small-scale events. This work also reveals that the same slide scarps can be reactivated
40 and generate slides with different flow behaviors.

41

42 **Plain Language Summary**

43 When studying large underwater landslides, determining whether what we see in our data was
44 created by one large landslide event or several smaller events is very difficult due to the
45 inaccessibility of the deep sea. But, being able to distinguish between different events and their
46 frequency allows for more accurate risk assessments. 40 years ago, a large landslide was
47 discovered in the northeast Atlantic, on the flank of an underwater plateau offshore of western
48 Ireland. Studies since its discovery have interpreted it as one large event. With present-day
49 technology and a higher resolution dataset, we have discovered that it is composed of several
50 landslides. The most recent, but very small and localized event, happened in the last 1000 years.
51 The one before is happened 10,000 years ago and it was the size of 680,000 Olympic-size
52 swimming pools. Around 22,000 years ago, a landslide 250 times bigger slid down the slope.
53 Two more similar size events happened more than 200,000 years ago, but the further back in
54 time we go the data resolution gets poorer. We think that the sizes of large underwater landslides
55 found in the world's oceans and lakes may have been significantly over-estimated, but their
56 frequency may have actually been under-estimated.

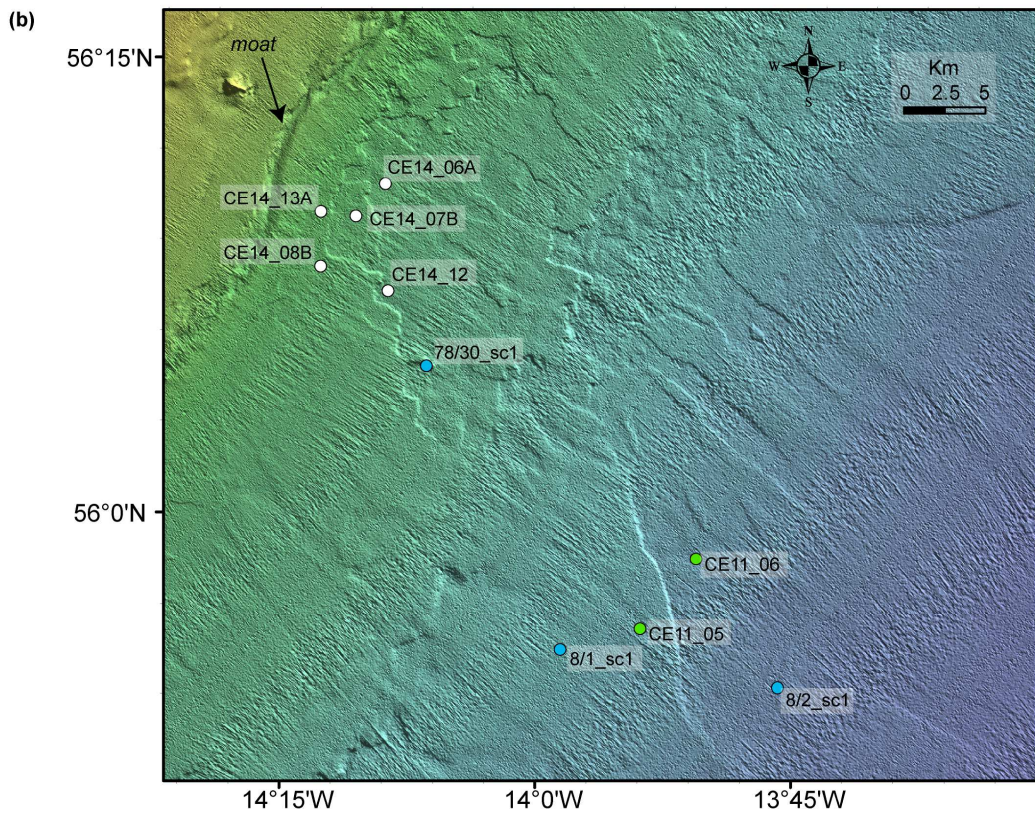
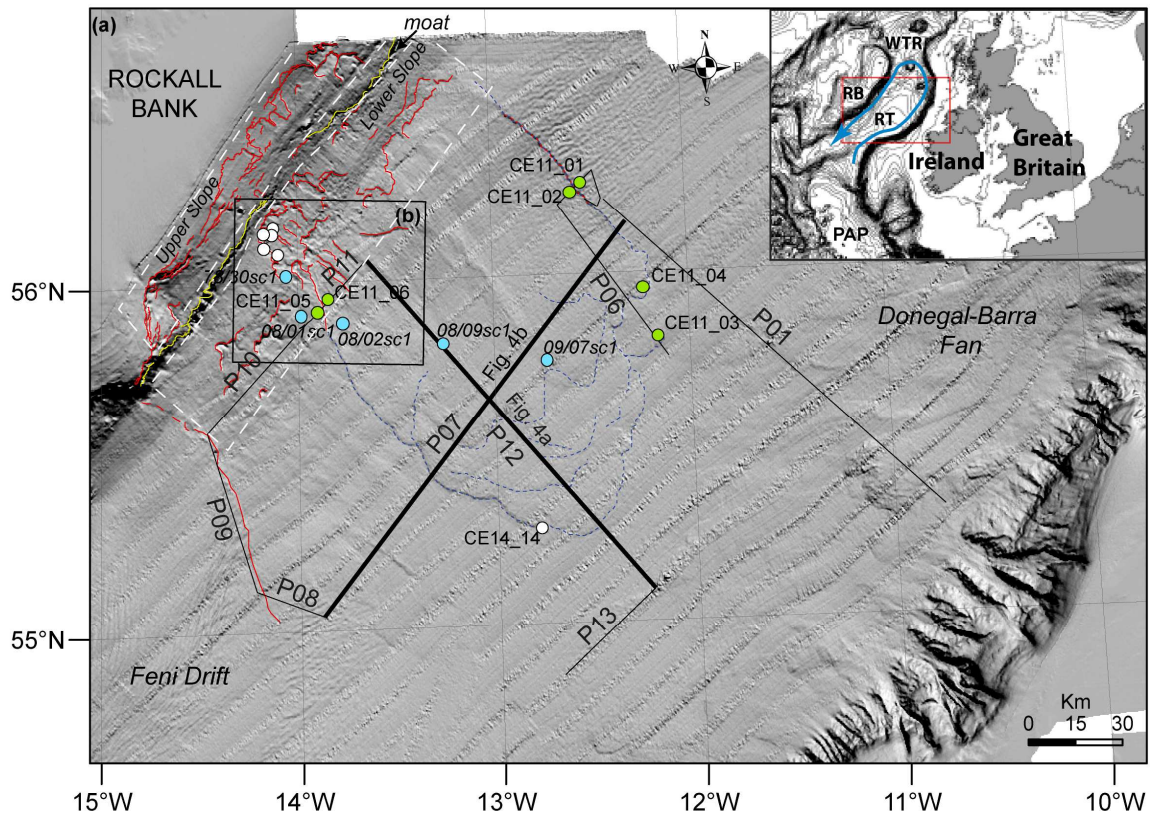
57

58 **1 Introduction**

59 Passive margins are often punctuated by large submarine landslides involving several 10s to
60 100s km³ of sediment affecting 1000s of km² of seafloor. Due to resolution limitations of seabed
61 bathymetric and seismic data and depth below seafloor restrictions of shallow coring systems, it
62 is often challenging to distinguish whether such large landslides took place as single large events

63 or as several phases that occurred sequentially over a period of time. Imaged slide scars and slide
64 deposits may be the cumulative effect of several episodes of slope instability in the same
65 location, but this can be especially difficult to determine if there are no obvious cross-cutting
66 relationships in the scarps or variable scarp degradation and sediment remoulding in the
67 bathymetric data and/or resolvable time in the seismic data between depositional lobes.
68 However, distinguishing between events and being able to calculate the volumes involved in
69 each episode, together with the interval between discrete failures, are of paramount importance
70 in geohazard risk assessment and in particular in modelling landslide-generated tsunamis. For
71 example, *Ward and Day* [2001] predicted tsunamigenic waves generated by a potential single
72 catastrophic failure of the west flank of the Cumbre Vieja volcano on La Palma in the Canaries
73 that could transit the Atlantic Basin and arrive at the American coasts with wave heights of up to
74 8 m. However, *Hunt et al.* [2011], using sedimentary records, demonstrated that collapses on the
75 northern flank of the adjacent island of Tenerife occurred as separate smaller events. They
76 showed that there is a markedly lower tsunamigenic potential where multistage retrogressive
77 failures occur, even where the time interval between individual failures is very short, in the order
78 of a few days [*Hunt et al.*, 2011].

79 This study focuses on the Rockall Bank Slide Complex (RBSC), a submarine slide complex
80 which lies on the eastern slope of the Rockall Bank offshore western Ireland, facing NW Europe
81 (Fig. 1). Bottom current activity and contourite deposition have been invoked as partially
82 responsible for the slope collapses here [*Elliott et al.*, 2010]. Buried basement scarps of the
83 Rockall Bank and contouritic deposition atop the scarps has been suggested to play an important
84 role in slope instability by generating differential compaction and pressure gradients, and



86 **Figure 1.** a) Shaded relief bathymetry map of the northern Rockall Trough offshore western
87 Ireland and data used in this study. The seismic profiles are shown in black and are numbered
88 P01-P13. The locations of CE11011 cores are indicated with green circles and of the CE14011 in
89 white circles. The turquoise circles show the locations of the Øvrebø et al. (2005) study. The red
90 lines show scarps associated with the RBSC, the yellow lines scarps associated with the moat
91 and the blue dashed lines depict the depositional lobes. White dashed boxes indicate the Upper
92 and Lower Slope regions after Georgiopoulou et al. (2013). PAP = Porcupine Abyssal Plain; RB
93 = Rockall Bank; RT = Rockall Trough; WTR = Wyville Thomson Ridge; b) A zoom in
94 bathymetric map on the location of the lower slope scarps and cores. Bathymetric data from the
95 INSS programme.

96

97

98 potentially directing fluid escape towards the seafloor [Georgiopoulou et al., 2013]. A study
99 using a traverse of four gravity cores across the RBSC determined with radiocarbon dating that
100 sliding took place during the last glaciation (~21.7 ka) [Øvrebø et al., 2005]. Georgiopoulou et
101 al. [2013] suggested that the RBSC probably occurred as a multiphase slope collapse involving
102 at least three episodes, with a potentially incipient or aborted fourth episode. That study relied on
103 indirect evidence from legacy 2D seismic reflection and the INSS (Irish National Seabed Survey)
104 bathymetric data from the scar area. In this paper we use the same bathymetric dataset but we
105 combine it with newly-acquired sediment cores, radiocarbon ages and newly-acquired 2D
106 seismic data from further downslope, in the depositional area of the complex to test the
107 hypothesis of Georgiopoulou et al. [2013] and distinguish the different slide episodes, evaluate
108 the volumes involved in each, and determine their timing and recurrence interval.

109

110 **2 Regional Setting**

111 Rockall Trough is an elongate, steep-sided, NNE-SSW trending intracontinental sediment-
112 starved basin located west of Ireland and the UK (Fig. 1). It is 200-250 km wide, with water

113 depths ranging from nearly 3000 m in the northern part to over 4000 m in the south where it
114 opens to the Porcupine Abyssal Plain (Fig. 1).

115 To the west, Rockall Trough is bounded by Rockall Bank, a structural high with an almost flat
116 plateau (0-2° slope) at <200-400 m water depths; Rockall Bank slopes to the east down to 2400
117 m in less than 90 km with gradients of 5-10°, in places exceeding 15° (Fig. 1).

118 The Irish continental margin lies at the boundary between the glaciated and the glacially-
119 influenced sectors of the European Atlantic margin [*Weaver et al.*, 2000]. During the last
120 glaciation the British Irish Ice Sheet (BIIS) was covering the entire island of Ireland and, at the
121 Last Glacial Maximum (LGM), 24 ka, it extended and was grounded close to the shelf edge
122 [*Peters et al.*, 2016]. Retreat of the ice margin began at 22 ka, but the ice shelf persisted for the
123 next 2500 years [*Peters et al.*, 2016].

124 Deep water masses in Rockall Trough flow northwards along its eastern margin, deflecting
125 anticlockwise at the steepening slopes of the Wyville Thomson Ridge and there flowing
126 southwards along the base of the Rockall Bank, excavating a moat at the base of slope (Fig. 1).
127 Bottom currents are responsible for the redistribution of sediments forming sediment drifts, most
128 notably the Feni Drift that occupies the western side of the trough (Fig. 1) and is mostly active
129 during interglacial periods [*Stoker*, 1998; *Stoker et al.*, 1998].

130 The floor of Rockall Trough is relatively smooth, gently getting deeper towards the southwest.
131 Major depositional processes that have dominated Rockall Trough are: the late Miocene to early
132 Pliocene contouritic Feni Drift; the Neogene to Pleistocene glaciogenic Donegal-Barra Fan
133 (DBF), a glacial trough mouth fan that drained the BIIS and occupies the northeastern margin,
134 with depositional lobes that extend towards the deeper parts of the Rockall Trough basin; the

135 RBSC that occupies the northwestern margin and truncates the Feni Drift and interacts with the
136 DBF lobes; and a series of channels that dissect the Irish slope but were mostly active during
137 glacial times [Elliott *et al.*, 2010; Sacchetti *et al.*, 2012a; Sacchetti *et al.*, 2012b; Stoker *et al.*,
138 1998]. Shallow cores from the deeper basin floor contain coarse sandy turbidites and contourites
139 alternating with hemipelagic layers [Georgiopoulou *et al.*, 2012]. Turbidite provenance analysis
140 suggests a switching of sources across the glacial-interglacial transition, with turbidites coming
141 from the Irish margin during the last glacial, via the DBF and the Irish slope channels, probably
142 generated by meltwater, and then, from Rockall Bank during the current interglacial, potentially
143 as flow transformation products from the Rockall Bank slope collapses [Georgiopoulou *et al.*,
144 2012]. The glacial hemipelagic intervals show the characteristic influence of ice rafted debris
145 [Georgiopoulou *et al.*, 2012].

146 Sedimentation rates were as high as 17.1 cm ka⁻¹ during the Holocene on the crest of the Feni
147 Drift but were lower (14.6 cm ka⁻¹) during the last glacial period, and significantly less prior to
148 that, averaging 5 cm ka⁻¹ for the Pleistocene [van Weering and de Rijk, 1991].

149 The RBSC truncates a field of sediment waves associated with the Feni Drift (Fig. 1). It also
150 excavated part of Rockall Bank and deposited sediment onto the floor of the trough [Elliott *et al.*,
151 2010; Flood *et al.*, 1979; Georgiopoulou *et al.*, 2013; Unnithan *et al.*, 2001] (Fig. 1). Scarps
152 associated with the RBSC have regional average gradients 30-35° and locally up to 70°
153 [Georgiopoulou *et al.*, 2013]. Volumes excavated from the entire scar have been estimated to be
154 between 260 and 760 km³ [Georgiopoulou *et al.*, 2013]. The glide plane for the RBSC is
155 believed to be the regional intra-early Pliocene C10 unconformity [Elliott *et al.*, 2010]. The
156 sedimentary sequence between C10 and the present-day seafloor outside of the main area of
157 failure (RTa in Stoker *et al.* [2001]) comprises alternating debris flow deposits and parallel-

158 wavy-bedded drift accumulations, locally disrupted by slope failure deposits [*Stoker et al.*,
159 2001].

160

161 **3 Data and Methodology**

162 Our study is based on 13 new multi-channel high-resolution seismic profiles (a total of c. 700
163 line-km), six new piston cores collected during RV Celtic Explorer cruise CE11011, five new
164 gravity cores collected during the SORBEH (Slope Collapses on Rockall Bank and Escarpment
165 Habitats) CE14011 expedition, four gravity cores from *Øvrebø et al.* [2005], and open-access
166 bathymetric data that had been acquired as part of the INSS programme between 2000 and 2001
167 on RV Bligh (Fig. 1). The multibeam bathymetry was collected using a Simrad EM120
168 multibeam echo-sounder with frequencies of 11.75–12.75 kHz. A detailed account on the
169 processing of the multibeam data can be found in *Sacchetti et al.* [2012a].

170 The seismic source used for acquiring the seismic data was a Mini-GI Gun. The gun was shot in
171 true GI-Gun mode with a volume of 0.2 l for the generator and 0.4 l for the injector. The
172 dominant frequency is ~200 Hz. The injector was triggered with a delay of 20 ms after the
173 generator to suppress the bubble signal in the recorded seismic data. The shooting rate was 9
174 seconds resulting in a shot point distance of ~20m at 4.5 knots boat speed. The gun operation
175 employed a high air pressure of 150 bar (2150 PSI). The data were received by a 187.5 m-long
176 120-channel streamer (Geometrics GeoEel); channel spacing was 1.56 m. Positioning was based
177 on GPS (Global Positioning System).

178 The processing procedure included trace editing, setting up geometry, binning at 5 m bin
179 distance, static corrections, normal moveout corrections, filtering, stacking, and finite-difference
180 time migration. A common midpoint spacing of 5 m was applied throughout. A constant velocity

181 of 1500 m/s was chosen for the NMO-correction and migration as the streamer was too short for
182 a velocity analysis. Poor weather conditions during acquisition caused a relatively high noise
183 level in the data but the careful data processing allowed to produce images with a good signal to
184 noise ratio. All seismic profiles are available in Supplement 1. The average depth of penetration
185 was 0.5 s but the signal is very attenuated beyond 0.3 s. With a sediment velocity of 1800-2000
186 m s⁻¹ the vertical resolution within those top 0.3 s is approximately 2.5 m. Seismic reflections
187 were picked and interpolated to produce surface maps in Kingdom Suite. The gridding algorithm
188 selected was Flex Gridding.

189 New cores from two different cruises are combined in this study (Supplement 3). The CE11011
190 (CE11) cores were collected using a Geo-piston corer with 110 mm-diameter and 6 m-length
191 barrels. Six cores were collected (Fig. 1) with average retrievals of 3.5 m, with the longest
192 retrieval being 4.29 m below the seafloor. The CE14011 (CE14) cores were collected using a
193 65mm diameter gravity corer with 3m and 6m-long barrels and average retrieval of 1 and 1.9 m
194 respectively.

195 The cores were first described visually for sediment structures, grain size, and colour
196 (Supplement 2). They were then logged for physical properties (gamma ray, p-wave velocity,
197 magnetic susceptibility and lightness) in a GeoTek Multi-Sensor Core Logger in split mode setup
198 in the Irish Sediment Core Research Facility at Maynooth University (Supplement 4). Selected
199 sandy samples were examined under a binocular microscope for bulk mineralogy comparisons of
200 different sandy intervals.

201 A total of 23 samples were taken for radiocarbon AMS (¹⁴C) dating and are supplemented by
202 three more from *Øvrebø et al.* [2005] (Table 1). The analysis was performed on pristine
203 planktonic foraminifera shells of mixed species as there was very little material for monospecific

204 picking. The dating was performed by the Poznań Radiocarbon Laboratory. The results were
 205 calibrated using Calib v7.0.4, based on the Marine 13 calibration dataset [Reimer *et al.*, 2013]
 206 (Table 1). A marine reservoir correction was applied based on data from the nearest location of
 207 $\delta R=53\pm 50$ (Castle Rock, North Channel – [Harkness, 1983]). Sedimentation rates are calculated
 208 between two samples taken from the same core or, where only one sample was taken from the
 209 core, between the top of the core taken to be Present Day, i.e. zero yrs BP and the depth of the
 210 sample. This was possible as there is no evidence of erosional features, no significant event beds
 211 or major facies changes between the sample depths and we are confident that the seafloor was
 212 recovered, usually obvious by the characteristic orange hue of oxidation.

213

214 **Table 1. Raw radiocarbon data, calibrated ages and resulting sedimentation rates.**

Core	depth downcore (cm)	Age 14C (BP)	Calibrated (BP)* (min-max)	Calibrated (BP) (average)	post-glacial sedimentation rates cm ka ⁻¹
CE11_02	210	15,200 ± 80	17,670 - 18,197	17,940 ± 260	11.7
CE11_03	10	2165 ± 30	1545 - 1838	1690 ± 150	2.45
CE11_03	22	7360 ± 40	7643 - 7915	7780 ± 140	
CE11_03	42	13,010 ± 70	14,310 - 15,161	14,740 ± 430	
CE11_05	73	24,960 ± 190	28,049 - 28,941	28,500 ± 450	2.56
CE11_06	134	13,830 ± 70	15,806 - 16,333	16,070 ± 260	12.3
CE11_06	203	18,420 ± 100	21,420 - 22,087	21,750 ± 330	
CE14_07A	65	10,160 ± 50	8941-9268	9120 ± 178	7.12
CE14_07A	129	19,590 ± 170	20,630-21,555	21,092 ± 462	samples bracket an erosional event
CE14_07A	156	25,020 ± 190	26,160-27,096	26,614 ± 454	
CE14_08B	20	19,150 ± 110	20,389-20,933	20,661 ± 272	sample within debrite clast
CE14_08B	40	>46,000			
CE14_08B	64	>46,000			
CE14_08B	64	>46,000			
CE14_08B	187	>46,000			
CE14_08B	192	>46,000			
CE14_08B	237	>46,000			
CE14_12	69	20,400 ± 120	21,697-22,378	22,037 ± 340	3.13
CE14_12	121	>46,000			
CE14_12	162	>46,000			

CE14_13A	29	9820 ± 50	8550-8969	8760 ± 209	3.3
CE14_13A	64	20,590 ± 120	21,928-22,569	22,248 ± 320	under erosional event
8/9_sc1	90	9500 ± 55	10,099 - 10,305	10,202 ± 103	8.82
8/9_sc1	120	>46,000			
9/7_sc1	160	20,540 ± 140	23,317 - 24,189	23,753 ± 436	6.75
9/7_sc1	200	18,800 ± 120	21,383 - 22,106	21,744 ± 361	under erosional event

* delR = 53 ± 50

Calibration Stuiver et al 1998

Between the lower two samples of CE14_07A there is a debrite, therefore no sedimentation rate between those two samples was calculated.

The top sample of CE14_08B was aiming to sample the base of a turbidite but it appears to have sampled a clast of the underlying debrite, therefore it is not used to calculate a sedimentation rate

The sample from CE14_13A at 64 cm dates the hemipelagic sediment at the base of a turbidite which was likely erosional, therefore it is not used to calculate a sedimentation rate.

215

216 **4 Results and interpretation**

217 4.1 Bathymetry

218 The planform morphology of the RBSC has been described in several previous studies [*Elliott et*
219 *al.*, 2010; *Flood et al.*, 1979; *Georgiopoulou et al.*, 2013; *Sacchetti et al.*, 2012a], so only a brief
220 summary is provided here with an emphasis on the lower slope and insights from the newly-
221 acquired seismic data. On the basis of different degrees and styles of deformation, the upper
222 slope where the scars of the RBSC are found, was divided into the Upper slope region and the
223 Lower slope region which are separated by an alongslope moat that strikes parallel to the base of
224 slope at approximately 1500 m waterdepth [*Georgiopoulou et al.*, 2013]. The Upper slope region
225 was further subdivided into the North, Central and South regions, which demonstrate very
226 different scarp characteristics; the North has rough-edged, arcuate scarps up to 150 m high,
227 whereas the South is dominated by cusped, bite-shaped, smooth-edged scarps also up to 150 m
228 high [*Georgiopoulou et al.*, 2013]. Strikingly different is the Central area, where there are at least

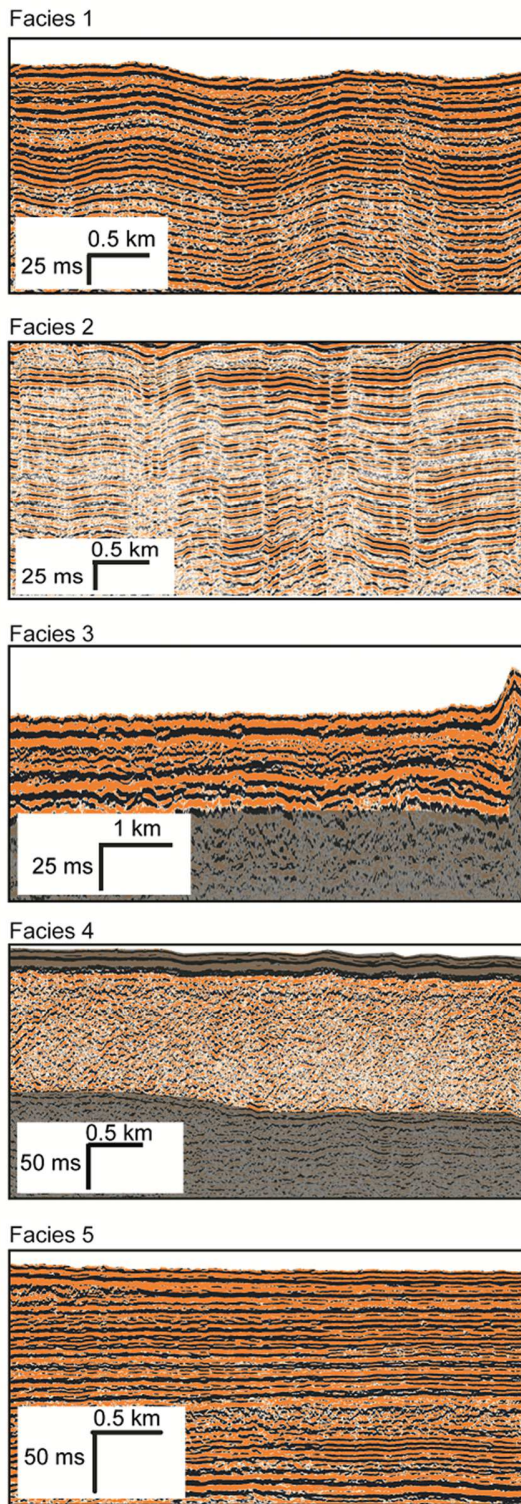
229 three scars, much shallower, up to 20 m high, separated by flat-topped ridges [*Georgiopoulou et*
230 *al.*, 2013]. The total width of the upper slope area that is affected by scarps is 120 km (Fig. 1).
231 Less than 5 km downslope of the moat, the Lower slope region is severely scarred by multiple
232 intersecting scarps (Fig. 1) [*Georgiopoulou et al.*, 2013]. Here, the RBSC is clearly still erosional
233 and its margins are defined by truncations of the sediment wave fields of the Feni Drift, along the
234 south and the north sidescarps (Fig. 1). Cores CE11_01 and _02 have targeted the northern
235 sidescarp, with CE11_01 serving as a reference core from the undisturbed seafloor and CE11_02
236 taken inboard of the scarp (Fig. 1a). There are a number of other sidescarps within this area,
237 downslope of the Lower slope region. Planar terraces at different stratigraphic levels can be
238 identified here and we observe a flow fabric downslope from them with elongate linear furrows,
239 ridges defining a conical-shaped erosional region opening downslope (Fig. 1b). The CE14 cores
240 targeted these terraces (Fig. 1b).
241 In the distal/depositional area the seafloor is occupied by a set of overlapping lobes, which at the
242 toe of the complex have sharp, up to 25 m high, frontal margins. Cores CE11_03, CE11_04 and
243 CE14_14 have targeted the terminations of these lobes (Fig. 1).

244 4.2 Seismic facies and their distribution

245 The newly-acquired multichannel seismic profiles provide a higher resolution of the sub-seafloor
246 sequence than previously seen on the legacy industry seismic profiles [e.g. *Elliott et al.*, 2010;
247 *Georgiopoulou et al.*, 2013]. The new data reveal that the acoustic character of the sediments is
248 highly variable both laterally and vertically. Five seismic facies have been identified and mapped
249 based on this newly-acquired dataset (Figs 2 and 3).

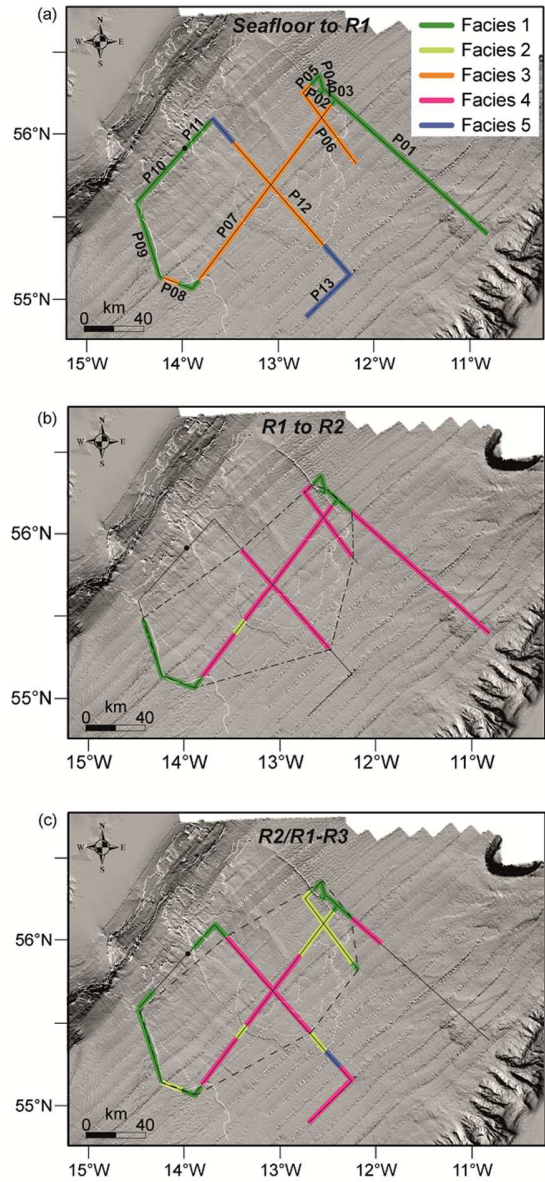
- 250 • Facies 1 comprises parallel, wavy, continuous reflections of moderate to strong
251 amplitude. The wavelength is between 1 and 2.6 km and the amplitude 5-10 m. This

252 facies, consisting of interbedded lithologies giving it its characteristic “striped”
253 appearance, is interpreted as the deposits of sediment waves created by bottom currents.
254 Their distribution coincides with sediment waves interpreted previously from bathymetric
255 and seismic data [*Elliott et al.*, 2010; *Sacchetti et al.*, 2012a; *Sacchetti et al.*, 2011], while
256 the scale range of approximately 1 km wavelength and 20 m height generally agrees with
257 the size of bottom current-related sediment waves [*Wynn and Stow*, 2002]. The sediment
258 waves are part of the Feni contourite drift and are



260 **Figure 2.** Seismic facies identified on the 13
261 seismic profiles.

262



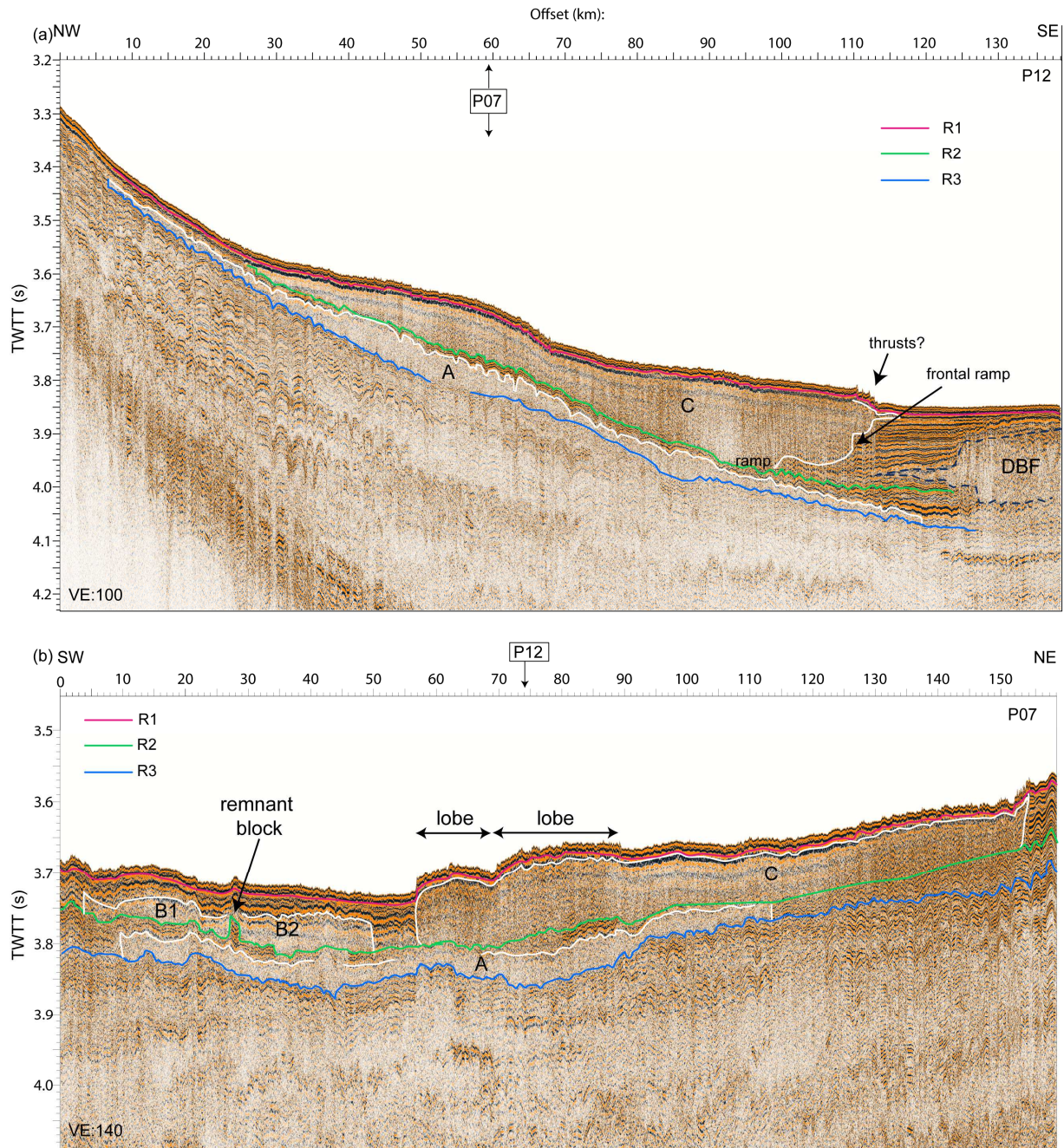
263

264 **Figure 3.** Distribution of the seismic facies
265 on the profiles at different stratigraphic
266 levels. The thin white lines show the scarps
267 and depositional lobes of the RBSC. (a)
268 Between the seafloor and Reflector 1, (b)
269 between Reflector 1 and Reflector 2 and (c)
270 between R2 (and where it missing R1) and
271 reflector R3. The dashed and dotted line in

272 (b) and the dashed line in (c) show the
273 mapped extent of R2 and R3 respectively
274 (see also fig. 5).
275

276 sharply truncated by the RBSC scarps [*Faugères et al.*, 1999; *Flood et al.*, 1979;
277 *Sacchetti et al.*, 2011].

- 278 • Facies 2 is characterized acoustically by weak to moderate amplitudes, and contains
279 parallel semi-continuous reflections. We interpret this facies also as generated by
280 sediment waves but within the scarps in the northern RBSC-affected area in the deeper
281 sedimentary sequence (Fig. 3c) which explains the weakening of the seismic amplitude.
282 They are sharply truncated to the southwest by a scarp. This relationship has implications
283 on the timing of the RBSC events and will be discussed further in section 4.5.
- 284 • Facies 3 shows sub-parallel, partly discontinuous, irregular reflections with high
285 amplitudes. We interpret facies 3 sediments as draping hemipelagic sediments, possibly
286 punctuated by turbidites, healing the topography left by the RBSC, as in most cases it is
287 found covering facies 4.
- 288 • Facies 4 is acoustically chaotic to transparent with few discernible structures or
289 reflections. Facies 4, which occupies mostly areas within the RBSC limits (scarps and
290 lobes) near the surface and at depth, represents deformed slope sediments. The acoustic
291 character demonstrated in this facies (transparent, chaotic reflections) is typical of slide
292 deposits [e.g. *Bull et al.*, 2009; *Sacchetti et al.*, 2012b]. The extent of this seismic facies
293 suggests that slide deposits are present beyond the confines of the RBSC limits as seen on
294 the seafloor, to the east (Fig. 4). This is coincident with the southwestern reaches of the
295 glacially-fed Donegal-Barra Fan that is sourced from the northeast Rockall Trough
296 margin and is almost entirely composed of debrites and mass transport deposits
297 [*Georgiopoulou et al.*, 2012b; *Holmes et al.*, 1998; *O'Reilly et al.*, 2007; *Sacchetti et al.*,
298 2011].



299
300

301 **Figure 4.** Seismic profiles (a) P12 along the length of the RBSC lobes and (b) P07 across the
 302 RBSC lobes (for location see fig. 1). Reflectors R1-R3 are shown in magenta, green and blue
 303 respectively. White lines are showing the upper and lateral limits of slide bodies A, B1, B2 and
 304 C. The profiles cross where indicated in each figure with an arrow.

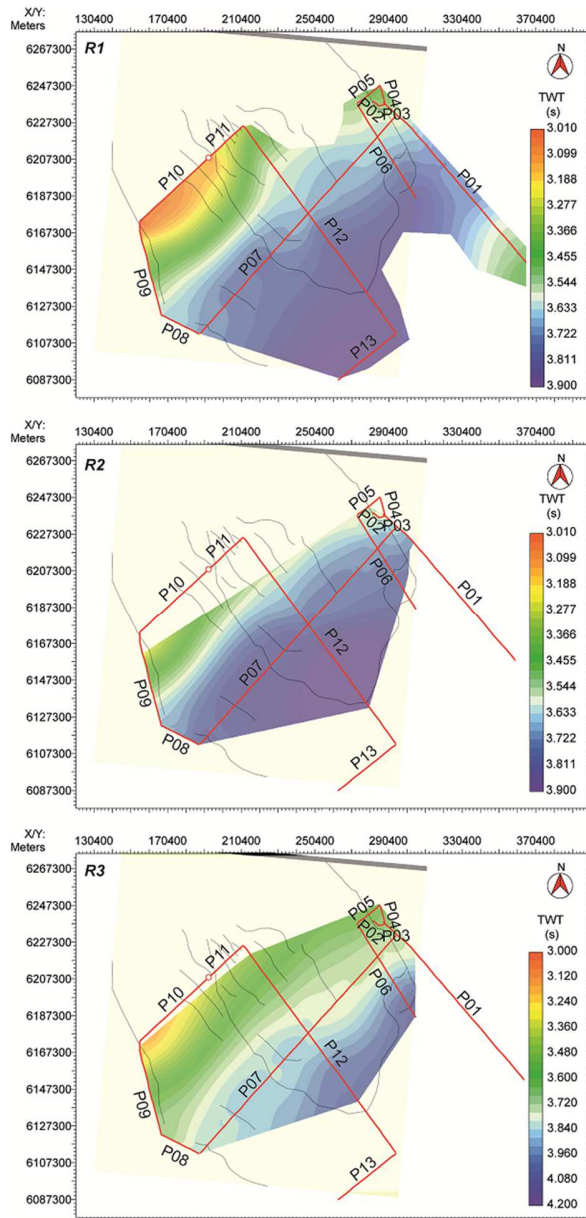
305 • Facies 5 shows parallel, mostly continuous reflections of high amplitude. Facies 5 is
306 similar to facies 1 in that it is characterized by a continuous layered seismic character.
307 However, it lacks the undulating character of facies 1. On the other hand, given the
308 similarity of the acoustic character, the lithologies are likely to be similar to those of
309 facies 1 and similarly with facies 3 are interpreted as hemipelagic sediments with
310 interbedded turbidites. Sediment cores from the near-surface that have been collected in
311 the area of facies 5 distribution confirm the presence of intercalated hemipelagic
312 sediments with sandy turbidite beds [*Georgiopoulou et al.*, 2010; *Georgiopoulou et al.*,
313 2012].

314 Three seismic horizons (R1-R3) have been mapped on most seismic profiles (Fig. 4), based on
315 their spatial continuity and their positioning relative to the acoustic facies distribution. Horizon 1
316 (R1) defines the surface post-failure sediments and has been mapped about 20-30 ms below the
317 seafloor throughout the survey. R1 is mostly continuous, only in places patchy, with low-to-
318 moderate amplitude. R1 is widespread and could be mapped on all profiles (Fig. 5a). The surface
319 sediments that lie between R1 and the seafloor are mostly high-amplitude, continuous reflections
320 of facies 1 and 5 outside the RBSC sidescarps, and mostly facies 3 within the scarps (Fig. 3a),
321 with the exception of an area of facies 1 that stretches within the scar near the base of slope,
322 along profiles P10 and P11 (Fig. 3a).

323 Horizon 2 (R2) is a moderate-amplitude, continuous reflector that is found in the central and
324 northern part of the survey (Fig. 5b). It is less widespread than R1, with clear terminations within
325 the study area; it shallows upslope and downslope towards R1 (Fig. 5b) and is sharply truncated
326 on profile P01 (Supplement 1). Between R1 and R2 the most prevalent facies is facies 4, at least

327 within the RBSC affected area, where it pinches out both upslope and downslope (Fig. 3b).

328 Outside the sidescarps,



329
330

331 **Figure 5.** Maps of the three reflectors. Note the widespread distribution of R1 in (a) and the
332 limited distribution of R2 (b) relative to both R1 (a) and R3 (c).

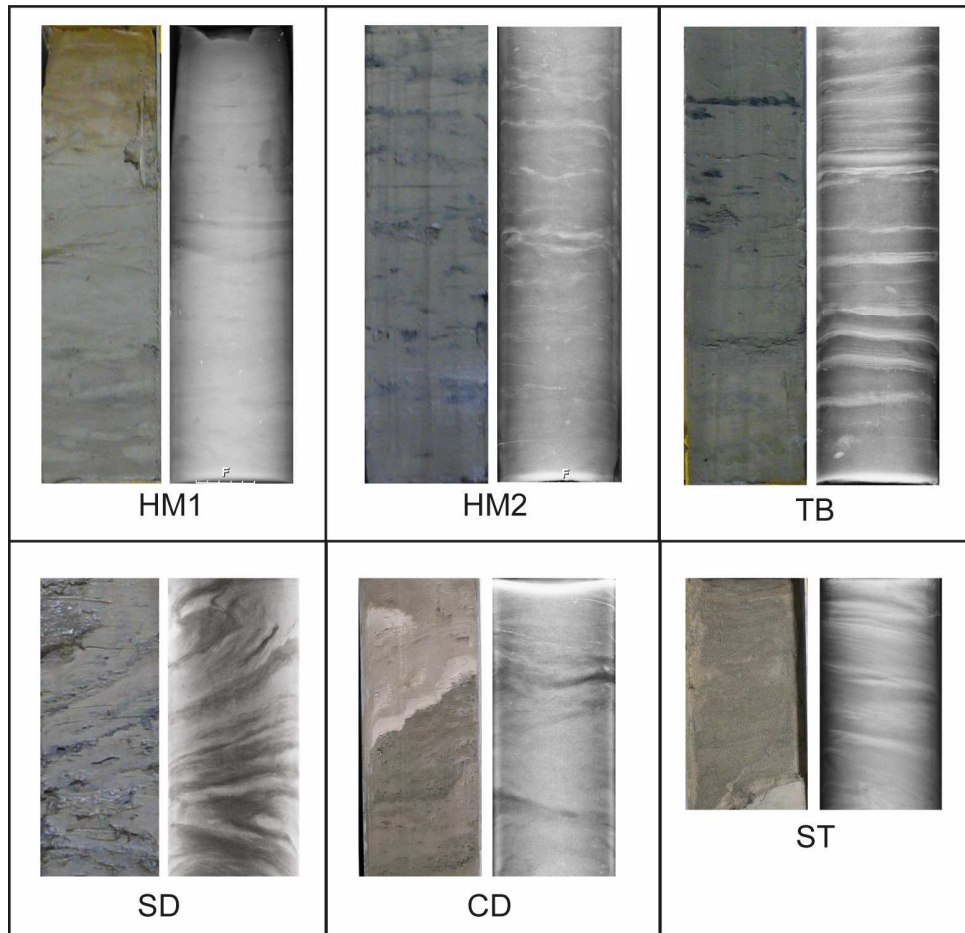
333 facies 1 is continuous from the seafloor down to the level of R2 and below (Fig. 4b). Facies 4 is
334 also found beyond the RBSC-affected area as seen on profile P1 which traverses the depositional
335 lobes of the Donegal Barra Fan (Figs 3b and c).

336 Horizon 3 (R3) is an irregular, moderate amplitude reflector that is fairly continuous and mapped
337 throughout most of the survey (Figs 4 and 5c). On profile P12 the quality of the seismic
338 deteriorates southeastwards and it is impossible to map the reflector. On profile P01 R3 is
339 abruptly truncated against facies 4 (Supplement 1). Facies 4 and 2 are found between R3 and R2;
340 facies 4 is located primarily in the central and southern area and facies 2 in the northern edge,
341 against the northern sidescarp (Fig. 3c). Outside the limits of the RBSC, facies 1 continues to be
342 dominant in the R2-R3 interval (Fig. 3c).

343 4.3 Sedimentary facies

344 The core data allow us to identify five main sedimentary facies. The criteria used are colour,
345 foraminifera content, sedimentary structures and physical properties (Fig. 6).

- 346 • HM are muds, further divided into two sub-facies; HM1, a light-coloured silty,
347 foraminifera-bearing mud and HM2, a dark-coloured, mottled, foraminifera-poor, clayey
348 mud. Their physical properties do not differ much; they show only very subtle differences
349 in p-wave velocity and gamma-ray density, while magnetic susceptibility seems to be
350 higher in HM2. Both subdivisions of Facies HM are found in all cores (Fig. 7).
- 351 • CD are clast-supported debrites and can be found in cores CE11_05 and 06, CE14_12,
352 _13A and 06A, and cores 8/9sc1 and 78/30sc1 (Fig. 7a).
- 353 • Facies SD represents deformed layers that may be sheared, folded or disrupted. For
354 example, there is a section of CE11_03, between about 80 cm to 175 cm downcore,
355 which appears deformed (Fig. 7b). The deformation cannot be attributed to coring



356

357 **Figure 6.** Sedimentary facies identified in the cores. Photo on the left and x-ray on the right for
 358 each of the sedimentary facies. See text for more details.

359

360 problems as it is not pervasive. However, it does not appear to be disintegrated and mixed
 361 as it maintains the original structures which in this facies appear deformed.

362

363

364

365

366

367

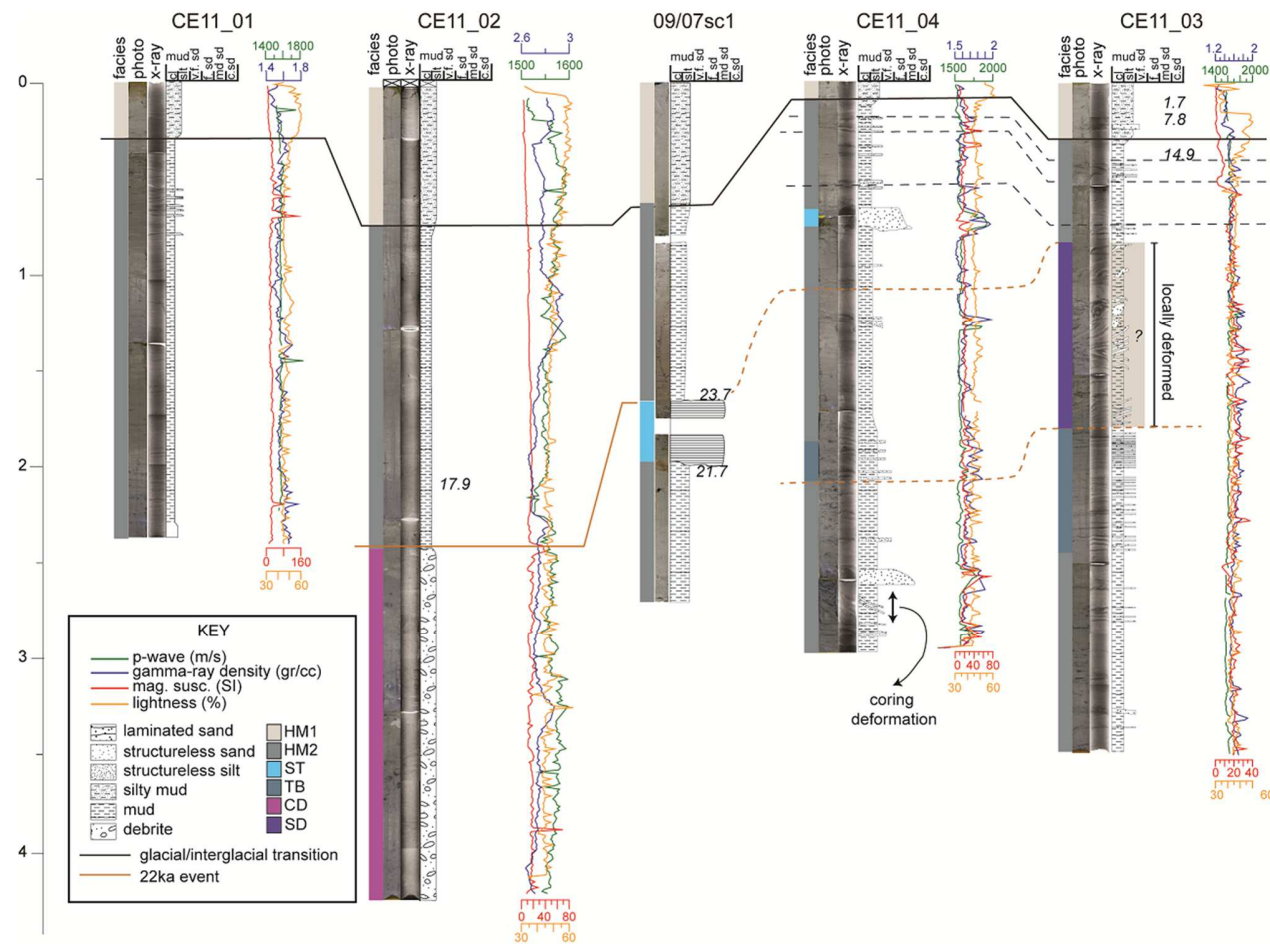
- ST are sandy layers (fine to medium sand), often fining upwards. In several of the cores this facies sits directly on top of CD. In most cases, the sandy layers appear laminated, better visible in the x-rays (Fig.6). Where lamination is not present the layers appear disturbed and fluidized, which may suggest destruction of the original structures, possibly because of coring [Jutzeler *et al.*, 2014]. They are characterized by increases in p-wave velocity, gamma-ray density, and magnetic susceptibility (Fig. 7).

368 • TB are thinly bedded silt-fine sand layers in dark clayey mud background (Fig. 6). Facies
369 TB is only seen in cores near the axis of the trough CE11_03, CE11_04 and CE14_14,
370 but is significantly thicker in CE11_03 (Fig. 7a). In this interval, the physical properties,
371 particularly the gamma-ray density and magnetic susceptibility, appear erratic, but the
372 pattern seems to suggest increases for both parameters in the coarser layers (Fig. 7a).

373 We interpret facies HM as background hemipelagic sediments with different degrees of
374 bioturbation, mostly by Zoophycos. The two subdivisions, HM1 and HM2, are similar to the GM
375 and BM facies reported in deeper water by [Georgiopoulou *et al.* [2012]. Like that study, and
376 based on radiocarbon dating (Fig. 7), we interpret HM1 to represent sediments deposited during
377 the current interglacial, which explains the higher foraminifera content and the light colour,
378 indicative of higher carbonate content and therefore higher productivity. The darker muds with
379 the black staining and paucity of foraminifera were deposited during the last glacial, confirmed
380 also by the dating (Fig.7). The age of the transition from the last glacial to the current interglacial
381 according to the radiocarbon data is 13 ka (based on CE11_03). We attribute the high degree of
382 bioturbation through HM1 is attributed to interglacial burrowing activity as evidenced by the
383 light grey HM1 mud that has been mixed with the darker HM2 mud.

384

385



388
389

390 **Figure 7.** a) Correlation panel of the lower slope cores, parallel to the flow axis; b) correlation panel of the cores along the northern
 391 edge of the RBSC. For each core we show the photo, x-ray (where available), lithological log, facies interpretation and physical
 392 properties (where available). Solid lines show confident correlations whereas dashed lines are inferred correlations and extensively
 393 discussed in the text. The ages (*italics*) are shown in years Before Present (BP). Insets A-D are blow-ups of the photo and x-ray from
 394 core CE11_05, and show in more detail the internal deformation in the debrite. Note the very small increase in density at 240cm

395 downcore in CE11_05; if two separate debrites were stacked the density at their contact would be expected to show a significant
396 increase to the right. The coring disturbance indicated in core CE11_04 took place during extraction of the core from the barrel.

397 Facies TB can be found only in CE11_03, _04 and CE14_14, which are the cores closest to the
398 axis of the Rockall Trough and nearest the Irish margin (Fig. 1b). We interpret this facies as fine
399 grained-turbidites originating from meltwater plumes from the BIIS that was covering the Irish
400 shelf to the east of the study area at the time [*Peters et al.*, 2016]. They correspond to the
401 turbidites that are found as thicker and slightly coarser sequences in cores more proximal to the
402 Irish slope [*Georgiopoulou et al.*, 2012], but they are not found in cores closer to Rockall Bank.
403 Rockall Bank was likely too distal for these turbidity currents and is also in shallower waters.
404 The clast-supported character of facies CD indicates this is a debrite composed of clasts of
405 multiple lithologies. This is the same character as reported by [*Faugères et al.*, 1981; *Øvrebø et*
406 *al.*, 2005].

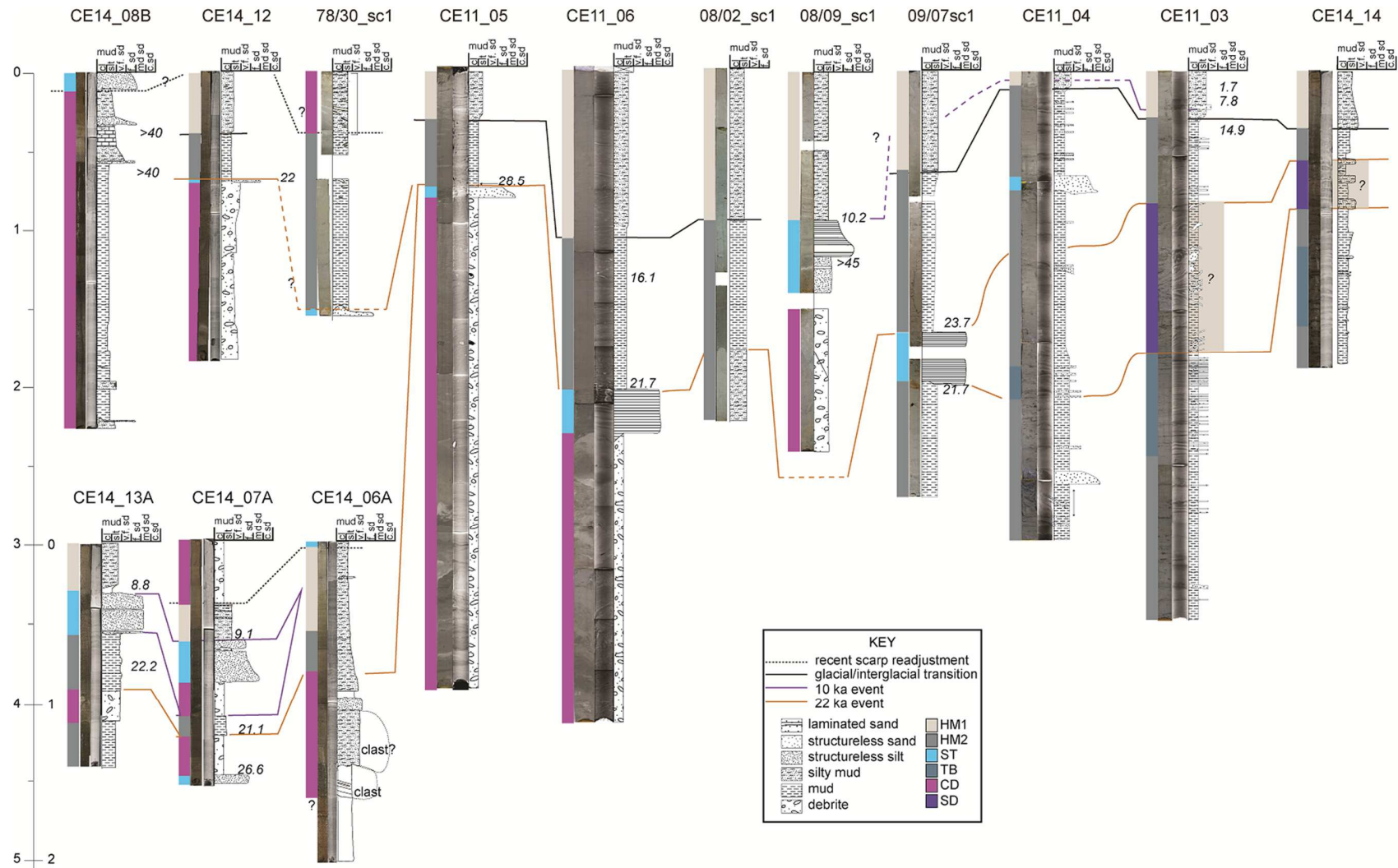
407 The section 83-240 cm in CE11_05 that corresponds to facies SD is remarkably different when
408 compared with the interval immediately below it in that it is not composed of multiple clasts.
409 Instead it appears similar to the glacial background sediments, but the bioturbation is deformed
410 there are some small (1-2cm diameter) clasts floating in the mud, and the x-rays show sheared and
411 inclined layers (Fig. 7a). These two sections could either be interpreted as two debrites that are
412 stacked, or infer that the interval 83-240 cm is a larger clast within the debrite. We prefer the
413 second interpretation as there is no sharp change in the gamma-ray density log (Fig. 7a), where
414 the second debrite would be shearing and depositing on top of the older one, causing
415 compression and/or eroding into deeper-buried strata with increased density.

416 The debrite is capped by facies ST in CE11_05 and _06 (Fig. 7a). We interpret this to be a co-
417 genetic turbidite that deposited from a more dilute suspended flow through debris flow
418 transformation or mobilized at the same time as the debris flow. This relationship was also
419 observed in the nearby gravity core 08/09sc1 of [*Øvrebø et al.*, 2005]. However the ages of the

420 deposits do not match (Fig. 8) and therefore cannot be correlated. They also correlate with the
421 debrite near the bottom of CE14_07A and the one in CE14_12 (Figs 7a and 8). About 30 km
422 laterally towards the east, neither the debrite nor the turbidite can be correlated into CE11_03
423 and _04, but stratigraphically they coincide with the top of the disturbed sequence in CE11_03
424 (Figs 7b and 8). This suggests that either the flow ceased close to the location of 09/07sc1 or that
425 it carried on beyond that location but just did not expand laterally towards the east.
426 Debrite/turbidite events occupying cores CE14_08B and 78/30_sc1 are difficult to correlate with
427 any of the other events and may represent a separate single event.
428 The timing of emplacement of these debrites and turbidites is discussed further in section 4.5.

429 4.4 Sedimentation rates

430 Sedimentation rates were calculated in intervals of hemipelagic sediments that are not punctuated
431 by any deposits that might have been erosional. Therefore, not all radiocarbon dates were used
432 (Table 1).
433 CE11_03 and CE11_05 show relatively slow sedimentation rates (ca 2.5 cm ka⁻¹) compared to
434 CE11_06 and CE11_02 (both about 12 cm ka⁻¹) (Table 1). We believe these differences can be
435 attributed to the location of the cores relative to the route of the bottom current, suggesting that
436 our cores straddle the boundary of the deep water mass that sweeps the base of slope of Rockall
437 Bank. Where the current effect exists, the sedimentation rates are larger, i.e. where cores
438 CE11_02 and CE11_06 were taken from, as opposed to the location of CE11_03 which is
439 beyond the effect of the bottom current. This interpretation is further corroborated by the
440 presence of sediment waves around CE11_02 and CE11_06, but not around CE11_03 (Fig. 1). A
441 problem that arises with this interpretation is that CE11_05 was taken only 5.5 km away from



442
443

444 **Figure 8.** Correlation panel of all the cores used in this study as compiled from figures 7a and b.

445 CE11_06, and yet the sedimentation rate is nearly an order of magnitude lower. Three reasons
446 can be invoked to explain this difference; (1) the dated sample from CE11_05 contained older
447 material either resulting from the heavy bioturbation evident on the x-ray images or because the
448 top of the sandy layer that forms the cap to the debrite was not completely avoided when
449 sampling; (2) the top one meter of the core is significantly compressed. However, the shape of
450 the trace fossils does not suggest any significant compression, so this possible interpretation is
451 ruled out; (3) sediment was preferentially depositing where there was more accommodation
452 space, and CE11_06 was taken from inside a scar, whereas CE11_05 just outside it. The
453 elevation difference between the two cores is 65 m.

454

455 4.5 Evidence of separate slide events and estimated volumes involved

456 The new high-resolution airgun data have revealed the distribution of the slide deposits (facies 4)
457 and the facies between them that allows the identification of at least three episodes of slope
458 instability. We assume that the geometry of each of the individual buried failure deposits is
459 lobate in shape with a NW-SE axis, similar to the lobes evident on the seafloor surface, in order
460 to estimate their volume and areal extent in the absence of a denser network of seismic lines.
461 On the basis of the seismic profiles, three distinct slide deposits can be identified (slides A, B
462 and C) (Fig. 4).

463 Slide A is found in the deepest section (between reflectors R2 and R3), separated vertically by
464 about 10 ms thick hemipelagic sediments (facies 1 and/or 5) from slide deposits B1, B2, and C
465 (Fig. 4). The slide deposits vary in thickness from 70 ms down to below the limit of resolution
466 (10 ms) and have an average thickness of 30 ms. Using an acoustic velocity of 1700 m s^{-1} for
467 moderately consolidated sediments [*Hamilton and Bachman, 1982*] this corresponds to slightly

468 less than 30 m. The area the Slide A deposits occupy is estimated at about 7,500 km² (Fig. 9)
469 indicating an approximate volume of ca 225 km³.

470 Slide B comprises two parts (B1 and B2) that are highly erosive, judging by the thickness of
471 truncated sediments against the edges of the deposits. B1 and B2 are separated laterally by a
472 segment of undisturbed seafloor sediments (Fig. 4b). While they may indicate two separate slide
473 events, they are found at the same stratigraphic level. This favours an interpretation where B1
474 and B2 are part of the same event that bifurcates around a remnant seafloor block or rafted block.
475 Interestingly, we observe a similar pinnacle-like feature on the seafloor vertically above the
476 remnant seafloor block (Fig. 4b). This pinnacle in fact corresponds to an elongate ridge that
477 strikes parallel to the flow direction. It is therefore likely that a similar ridge caused slide B to
478 bifurcate around it. Slide B is 20-60 ms thick, on average 35 ms, which with an acoustic velocity
479 of 1600 m s⁻¹ for less consolidated sediments than slide A [*Hamilton and Bachman, 1982*] as this
480 is at shallower stratigraphic level, corresponds to ~30 m thickness. The extent of slide B is more
481 limited than slide A, at 4,500 km², and we estimate the volume to be ca 125 km³.

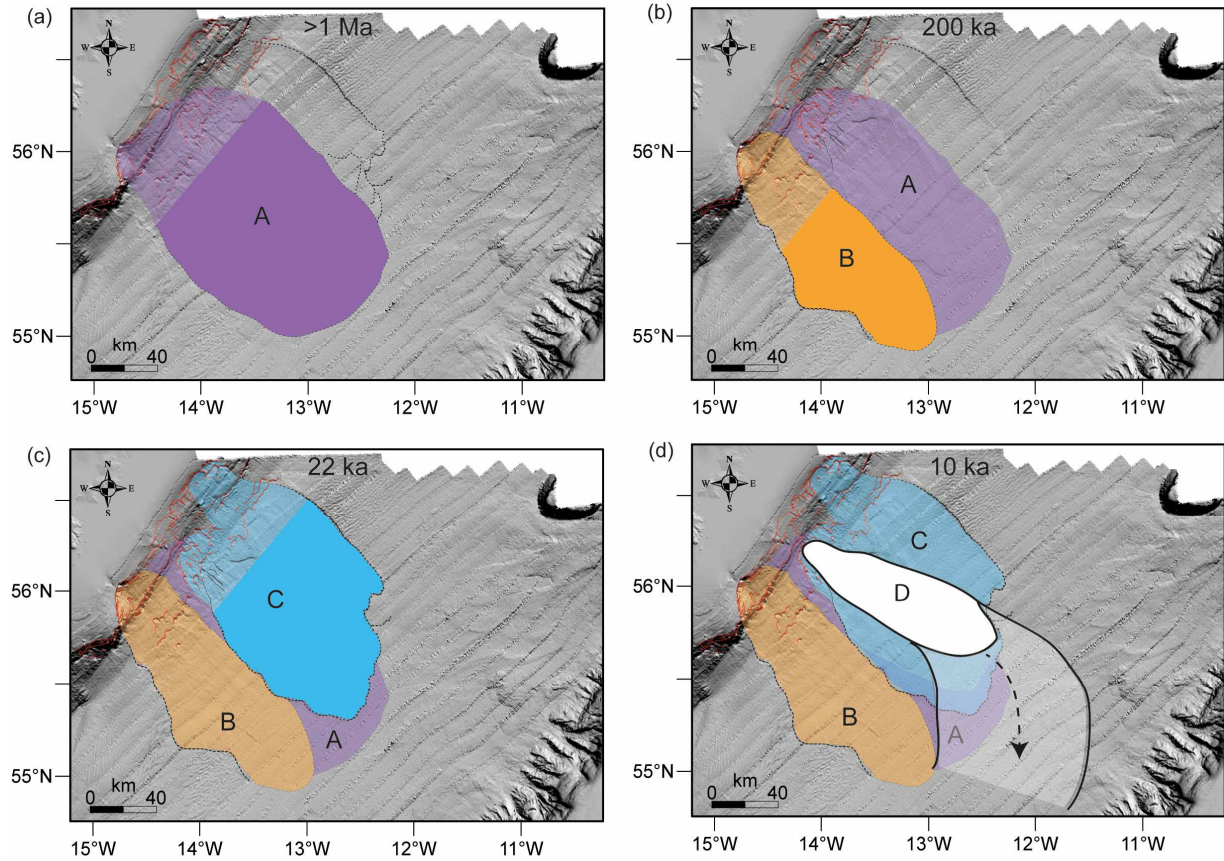
482 Slide C is characterized by variable internal acoustic character, probably due to different degrees
483 of disintegration and potentially variable lithology (Fig. 4). This deposit is thicker than slide B, at
484 about 120 ms maximum thickness, but has an average thickness of 75 ms, or 60 m (assuming the
485 same acoustic velocity of 1600 m s⁻¹ as for slide B). The cores sample the top part of this deposit
486 but do not penetrate it fully (orange line in figs 7 and 8 mark the top of the deposit), Slide C is
487 linked with the lobes that extend on the seafloor downslope of the North Upper Slope scar and
488 the Lower Slope scar (after *Georgiopolou et al. [2013]*) and we calculate its extent at 6,600 km²
489 (Fig. 9) and its volume at ca 400 km³, making slide C the most voluminous of the three slides.

490 A fourth event, slide D, is only identifiable in the cores as it is too thin to be resolved by the
491 seismic data (purple line in Figs 7 and 8). In some cores we only observe a fining upward
492 turbidite (medium to fine sand) (e.g. cores 08/09_sc1, CE14_13A), while in others the turbidite
493 caps a clast-supported debrite (facies CD) (e.g. cores CE14_07A, CE14_06A and possibly
494 CE14_08B). It occupies the central downslope area according to its distribution in the cores (Fig
495 9d). Its deposits suggest that it was a dilute event (further discussion in section 5.1) that
496 generated a turbidity current which flowed ESE and was directed southeastward towards the
497 deepest part of the Rockall Trough, following the seafloor topography (Fig. 9). The average
498 thickness of the event in the study area is 30cm and it occupies an area of 4000 km² which gives
499 a volume of at least 1.2 km³. The volume of the turbidite, which is on average 10cm thick and
500 occupies an area of nearly 5000km², adds another 0.5 km³.

501 The volume of the RBSC was previously calculated by *Georgiopoulou et al.* [2013] based on
502 estimates of the missing sediments from the scars on the Rockall Bank slope. They used two
503 approaches: a “conservative” approach, where the volume of evacuated sediments was based on
504 connecting the scarps by straight, planar surfaces and a more “generous” approach, where the
505 volume of evacuated sediments was calculated by connecting the scarps with dome-shaped
506 surfaces. The two approaches generated volumes that vary from 265 to 765 km³ of missing
507 sediments. The present study indicates the total volume of the four slide deposits amounts to ca
508 750 km³, which is very close to the “generous” volume of *Georgiopoulou et al.* [2013]. This also
509 suggests that the “generous” approach, where a mounded contouritic morphology on the Rockall
510 Bank slope was considered prior to slope collapse, is more realistic than the “conservative”
511 approach in estimating the missing volumes from the scars. However, it should be noted that one
512 of the slides, Slide B, was highly erosive (as discussed above) and therefore the volume of the

513 deposits should exceed the volume of the evacuated sediments, but it is difficult to estimate by
 514 how much.

515



516
 517

518 **Figure 9.** Inferred distribution of slides A, B, C and D based on the seismic and core data as well
 519 as the seafloor lobes as expressed on the bathymetry, in the order they took place. The lighter
 520 shaded area is the interpreted evacuation area, whereas the darker shaded area is the interpreted
 521 depositional area (for each panel the entire area of the earlier slides is lightly shaded). The arrow
 522 in (d) indicates the direction of flow of the Slide D turbidity current and the transparent white
 523 area indicates the extent to which it spread.

524 4.6 Emplacement age of RBSC events

525 We have calculated a sedimentation rate of about 12 cm ka^{-1} for the last 20 ka for the Rockall
526 Bank slope, and about 2.5 cm ka^{-1} for the deeper Rockall Trough, away from the influence of
527 bottom currents (Table 1). In order to estimate the ages of the older events we have extrapolated
528 the Rockall Bank sedimentation rate back, assuming constant sedimentation rates, recognizing
529 the uncertainties and potential errors in this approach, particularly the deeper in the record we
530 extrapolate where climatic changes would have affected sedimentation rates significantly. In
531 addition we are considering average radiocarbon ages rather than ranges which also contains
532 errors.

533 Slide A is the oldest event. It is difficult to estimate its age with any confidence as there is no
534 way of knowing how much sediment has been removed through erosion by Slides B and C that
535 overlie it. All we can say confidently about Slide A is that it is older than horizon R3 which is
536 probably a few Ma old given the thickness of acoustic facies 5 and the sedimentation rate we
537 have calculated and employed. However, it would be unreasonable to use the same
538 sedimentation rate for the length of period it would have taken to deposit this amount of
539 sediment considering how variable sedimentation rate can be over time.

540 The southernmost deposit, Slide B, is buried under ca 24 m of sediments, which with the above
541 sedimentation rate for the Rockall Bank slope (12 cm ka^{-1}), yields an estimated age of 200 ka.
542 Slide C appears to have deposited at approximately the same stratigraphic level as Slide B, on
543 top of Horizon R2 and adjacent to Slide B (Fig. 4b), probably due to the seafloor topography that
544 Slide B created and then Slide C was routed through it. However, Slide C appears on seismic
545 profiles to be either exposed at the seafloor (Fig. 4) or if there is a drape on it, it is thinner than
546 the vertical seismic resolution (ca 8 m). By assuming a drape thinner than 8 m and using a
547 sedimentation rate of 12 cm ka^{-1} we can estimate that slide C is younger than approximately 70

548 ka. A sub-bottom profile shown in *Georgiopoulou et al.* [2013] (their figure 5) shows recent
549 slide deposits inside the Upper North Slide scar, upslope of Slide C. Their results indicate that
550 either Slide C is actually significantly younger than 70 ka or that there has been another, very
551 recent slope collapse in the same area that is not resolved on the seismic data. Indeed, even high-
552 resolution Pinger data with 1m vertical resolution do not show slope collapses in the area
553 younger than slide C [*Sacchetti et al.*, 2012a]; see their figure 5). However, our core data clearly
554 demonstrate that there has been a more recent failure, slide D, that was deposited only about 0.5
555 m above slide C and therefore could not be resolved even by the pinger high-resolution data
556 (Figs 7a and 8). The only way to distinguish and establish the distribution of slides C and D is
557 based on the presence (or absence) of the youngest event in the cores.

558 Core CE11_02 suggests there has been an event, at 20,850 cal BP (which is the age of the sample
559 taken 35 cm above the top of the debrite, 17,940 cal BP, plus the 2910 years that it would have
560 taken to deposit the 35 cm at 12 cm ka⁻¹ sedimentation rate). This 20,850 cal BP event is not
561 found in CE11_01, which was collected from the undisturbed seafloor adjacent to the slide side
562 scarp to the north. The event is found in CE11_06 where it has a very similar age of 21750 cal
563 BP. The sandy turbidite that caps the debrite in CE11_06 is also found in CE11_05, although the
564 age in core CE11_05 suggests that this layer of sand is older (28,540 cal BP) which would make
565 them uncorrelated. However, this sample was taken from a part of the core that appears to be
566 heavily bioturbated (Fig. 7a) which could have mixed in older material. We suggest that this is
567 the same sandy layer based on its stratigraphic position downcore and the physical properties
568 (Fig. 7a). We considered whether the sandy layer in CE11_04, between sections 1 and 2, also
569 correlated with the sandy layer in CE11_05 and _06, but the physical properties and mineralogy
570 differ (Fig. 7a); in CE11_05 and _06 the sand is foraminifera-dominated and contains rounded

571 and angular lithic grains, whereas in CE11_04 there are very few foraminifera relative to the
572 clastic material which is dominated by glassy angular quartz and dark green lithic fragments.
573 There are also significant differences in the physical properties; crucially the magnetic
574 susceptibility that is a reflection of mineralogy, is higher in CE11_05 and _06, whereas the p-
575 wave velocity and gamma-ray density are higher in CE11_04. Therefore we do not believe the
576 sandy layer correlates across into CE11_04. Core CE14_12 contains a debrite capped by a very
577 thin sand layer dated at 22,037 cap BP which correlates well with the other cores. The same
578 event appears in core 09/07_sc1, dated at 21744 ka [Øvrebø *et al.*, 2005] which is also in very
579 close agreement with the other ages and with an error range that makes them overlap. Cores
580 CE11_03 and CE11_04 contain no debrites at the appropriate stratigraphic interval, but the
581 sedimentary sequence from about 1 m downcore, which is where a slide C deposit would have
582 been anticipated, appears disturbed in CE11_03. This could have resulted from slide material
583 buttressing against and ploughing through the seafloor further upslope and causing in situ
584 deformation of the seafloor. Alternatively, it could be due to the coring procedure, which is not
585 uncommon with piston coring [Jutzeler *et al.*, 2014] but the deformation we see in this interval
586 does not match any of the previously described types, i.e. it is not limited to the sandy intervals,
587 there is no arcuate warping of the layers or extension and breaking of the muddy interval. Instead
588 the deformation is consistent with plastic deformation of soft sediments as it would appear in a
589 debrite only the stratigraphic order of the layers has not been altered. As seen on the bathymetric
590 data, cores CE11_03 and CE11_04 were taken from the edges of depositional lobes of Slide C,
591 i.e. very close to causes of seafloor disturbance. Based on the correlation of the sandy turbidite
592 layer across CE11_05 and _06, it appears that the 22 ka event that generated the debrite/turbidite
593 seen in CE11_05 and _06, may have been responsible for the deformation seen in CE11_03. A

594 similar character is observed at a similar stratigraphic position in core CE14_14 that was taken
595 from the edge of the lobe on the southern side of the complex (Fig. 7a). 08/02_sc1 does not have
596 a deposit that correlates with this event. Nevertheless there is a very sharp contact between
597 contrastingly different hemipelagic sediments (on the basis of colour and lithology) (Fig. 7a).
598 This surface could only have been created by an erosional event and given its stratigraphic
599 position we assign it to the 22 ka event. Given the coincidence of the distribution of the
600 debrite/turbidite in the cores and the distribution of Slide C on the seismic, we believe that slide
601 C is the 22 ka event.

602 Across the cores from the Lower slope region and in the middle of the slide complex we found a
603 younger debrite-turbidite pair higher in the stratigraphy (Slide D). This event is encountered in
604 cores CE14_13A (dated 8760 cal BP) and CE14_07A (dated 9120 cal BP), in 08/09_sc1 (dated
605 10,202 cal BP) from *Øvrebø et al.* [2005] and possibly in CE11_03 as a thin turbidite, without a
606 debrite. The age of this event has been determined to be around 10 ka. Absence of this deposit
607 from CE11_05, CE11_06, 08/01_sc1 and 08/02_sc1 (Fig. 8) suggests that this flow followed a
608 narrow ESE trajectory. This event coincides stratigraphically with the T2 turbidite described by
609 Georgiopolou et al. (2012) in the deeper Rockall Trough.

610 There appears to be a recent debrite near the top of CE14_07A as well as the top of 78/30_sc1
611 and a turbidite at the top of CE14_06A, while the entire CE14_08B consists of a debrite deposit
612 capped by a turbidite that is at the top of the core. It is hard to determine whether the deposits in
613 CE14_08B and 78/30_sc1 correlate with the 10 ka event or the even more recent event. This
614 latest event does not have a large extent and is not identified in cores further away from the
615 scarps, so it is likely that it is the result of scarp spalling and small equilibrium adjustments (e.g.
616 [*Carter et al.*, 2018]).

617

618 5 Discussion

619 5.1 Styles of mass transport

620 Several different types of deposits have been identified in the RBSC, pointing to a wide range of
621 flows in the spectrum of sedimentary flow processes, from dilute to cohesive flows. Core data
622 allow us to assess and compare the flow processes in the last two phases of slope instability in
623 the RBSC, during slides C and D.

624 Slides A and B, being buried deep below the seafloor, and in the absence of their sedimentary
625 record in the cores, cannot be assessed for flow type save for their acoustic record. The top of
626 Slide A appears blocky. However, the large runout and then thinness of the deposit suggest that it
627 must have transformed downslope to a more fluid flow that allowed it to spread laterally.

628 Similarly, slide B appears to have been blocky, but less widespread and thicker with pronounced
629 and steep lateral margins. From these characteristics we infer that slide B was probably more
630 concentrated and perhaps flowed more plastically like a debris flow that halted its movement *en*
631 *masse*, freezing in place. A dilute component that would have deposited a turbidite further
632 downslope cannot be dismissed, but there is no evidence for it with the available data.

633 Slide C appears to have been a bimodal flow, comprised mostly of a cohesive clast-rich debris
634 flow and an accompanying dilute cloud or tail that deposited a thin turbidite as the flow was
635 waning. The turbidity current could have been either high-density or low-density as both can
636 deposit laminated sands [*Sumner et al.*, 2012], which is what has been retrieved in the cores. The
637 runout of the turbidity current was not significant, as we do not encounter it in cores beyond the
638 limits of the slide [*Georgiopoulou et al.*, 2012]. The top of Slide C appears smoother than Slides
639 A and B and we interpret this to mean that the character of this flow was less blocky and maybe

640 more plastic. Similar to slide B, the toe of slide C appears thick, thicker than the body of the slide
641 (Fig. 4), and set within stratified pre-existing sediments as if it buried and confined itself,
642 ploughing through the seafloor. Small-scale thrusts are likely present at the toe (Fig. 4) lending
643 further evidence towards a self-confining type of flow, but not to the extent previously reported
644 for self-confining submarine landslides [*Frey Martinez et al.*, 2005]. Further corroborating
645 evidence comes in the form of the sheared section in core CE11_03 that appears as though in situ
646 layers have been locally deformed, possibly due to the lateral pressures emanating from the toe
647 of the slide ploughing through the adjacent seafloor. Different scenarios for modelling of slide C
648 to match the deposits as seen on the bathymetric data reveal that the best fit resulted when a
649 Bingham rheology was adopted with either a velocity-dependent term or with basal frictional
650 properties [*Salmanidou et al.*, 2018].

651 Slide D on the other hand, appears to have been more dilute, perhaps fully transformed into a
652 turbidity current as indicated by the deposit found in the cores. However, in spite of its dilute
653 nature, this flow did not spread laterally much but did have a long runout and extended mostly
654 downslope as it can be found in a deeper part of the basin [*Georgiopoulou et al.*, 2012]. These
655 characteristics suggest that Slide D was more rapid and more focused than the previous episodes
656 of failures as it is found along a relatively narrow, elongate axis (Fig. 9d).

657 Finally, the latest episode was probably generated by minor secondary scarp spalling that did not
658 produce a large event, and the deposits have not gone far from the scarp source. The timing of
659 this event is estimated to be some time in the last millennium as there does not seem to be any
660 substantial drape covering it.

661 The sequence of events described here based on the depositional data is in general agreement
662 with the sequence of events proposed by *Georgiopoulou et al.* [2013]. However, the present

663 study reveals that these events took place over a considerable period of time. This has also
664 demonstrated the predisposition of the slope for ongoing slope instability and repetitive failure.
665 For example, Slides A and B appear to originate from the same source, even though Slide B was
666 almost half the size of A, but it may have resulted from retrogression of the Slide A scarp.
667 Attempts to model the flow behaviour of slides A and B, using the same approach as for slide C,
668 demonstrated that this was not possible and the modelled deposits mapped beyond the actual
669 ones [*Salmanidou et al.*, 2018]. This was attributed to potentially different rheological properties
670 [*Salamanidou et al.*, 2018]. Therefore, the assumption that slide events that occur in the same
671 area and as a result should have the same lithological characteristics, and by extension
672 rheological characteristics, is wrong, at least for this case study, as demonstrated by *Salmanidou*
673 *et al.* [2018] and by the different deposits we find in the cores in this study.
674 We also observe that slide events become more frequent in more recent geological time. This
675 does not necessarily reflect an increased rate of slope failure but is more likely a reflection of the
676 increased resolution closer to the seafloor. This could indicate that the thick deposits identified in
677 the deeply buried slides may comprise the composite products of a number of smaller stacked
678 events rather than the result of single large events.

679

680 5.2 Wider implications

681 Early work suggested that the RBSC probably occurred as a single event [*Faugères et al.*, 1981;
682 *Flood et al.*, 1979]. *Georgiopoulou et al.* [2013] examined the scarp morphology at the headwall
683 of the complex and suggested that there may have been several episodes given that the
684 “freshness” or angularity of the scarps varies across the slope, but they were unable to draw any
685 conclusions regarding the timing of events, other than that there were likely to have been

686 significant hiatuses between events as seafloor modifications and healing appeared to have taken
687 place over the older events.

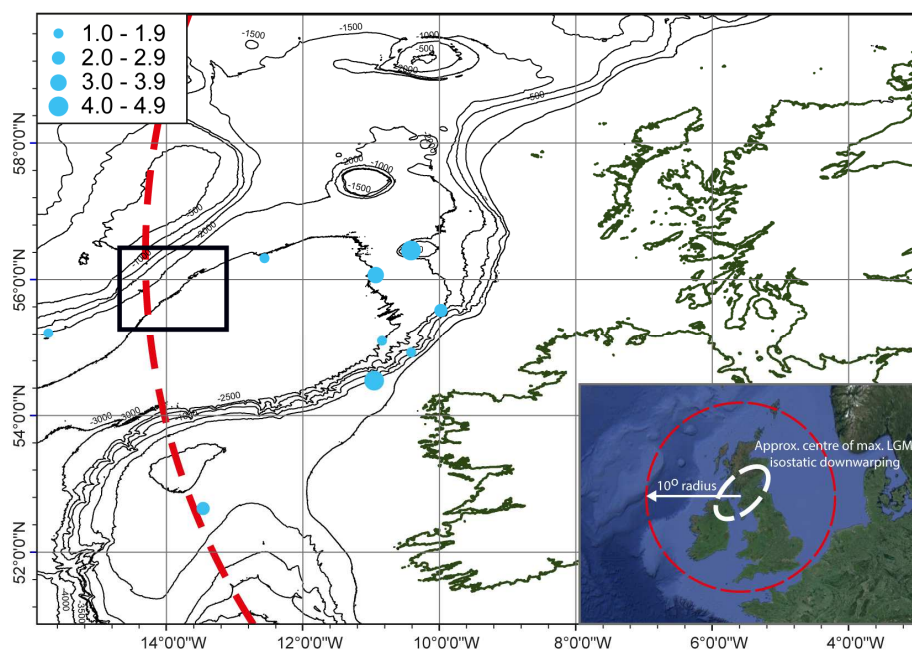
688 In this study, with access to new high resolution seismic data and a large number of new cores
689 from the depositional area, we are able to confirm the multi-stage nature of RBSC and cast new
690 light on the emplacement ages and timing between separate events. We are thus able to
691 demonstrate the long history of instability of the Rockall Bank eastern slope. The youngest slide
692 event, that appears at the top of a limited number of cores, likely took place within the last 1000
693 years but it appears it was very small and did not affect a significant area. The 10ka event (Slide
694 D) was a relatively small event in terms of volume ($<2 \text{ km}^3$) but had a very long runout. Slide D
695 was nowhere near as voluminous as Slides A, B and C, but it is significant nonetheless and
696 demonstrates that more events of these dimensions may be “hidden” in the resolution of the
697 seismic data which has implications for risk assessment studies that consider the repeat interval
698 of submarine slope failures.

699 The youngest of the large events (Slide C) appears to coincide with the Last Glacial Maximum
700 (LGM), the height of the last glaciation [*Clark et al.*, 2012]. During glacial periods, when the sea
701 level fell, continental margins experienced increased terrigenous input as much of the shelf was
702 exposed and became a sediment source [*Johannessen and Steel*, 2005]. A lower sea level may
703 have exposed part of the Rockall Plateau as a small island, but it could not have been large
704 enough to generate the required large amounts of sediment input as it is not connected to a land
705 mass and its dimensions are limited. Additionally, the predominant sediment supply for Rockall
706 Bank, as evidenced by seismic profiles and cores, came through bottom currents running parallel
707 to the slope [*Georgiopolou et al.*, 2013; *O'Reilly et al.*, 2005; *Øvrebø et al.*, 2005; *Stoker et al.*,
708 2005]. However, bottom currents in Rockall Trough are considered to have been slow during

709 glacial times, with seafloor sediment waves barely affected and with minimum winnowing
710 power [Howe, 1996]. Previous studies have suggested a combination of rapid sediment
711 accumulation from bottom currents on top of steep basement scarps and slope undercutting by
712 the bottom currents as instability triggering mechanism for this slope [Elliott *et al.*, 2010;
713 *Georgiopoulou et al.*, 2013]. However, given the timing of Slide C at 22ka, could this
714 mechanism have been a primary trigger? It is likely that the slope reacted with some lag time and
715 currents had already destabilized it prior to their weakening and a ground vibration acted as the
716 final trigger. Another factor that may have contributed is fluid seepage to the seafloor. A number
717 of closely-spaced faults can be seen in the seismic profiles (Fig. 4a) that may have also
718 facilitated fluid flow to the seafloor but no direct evidence for fluid seepage can be seen on this
719 resolution of seismic or the bathymetry.

720 At 22 ka the British Irish Ice Sheet was starting to decline [Clark *et al.*, 2012]. Models of
721 isostatic loading for the Eurasian Ice Sheet that includes the British Irish Ice Sheet, show that
722 isostatic loading did not affect Rockall Bank [Patton *et al.*, 2016] that lies just at the limit of the
723 affected region (see fig. 12 of Patton *et al.* [2016]). Isostatic unloading readjustment is
724 experienced in an extensive area beyond the centre of the ice load, which is about 10° of
725 longitude (roughly 1000 km) for the BIIS-sized ice load [Lambeck, 1996]. The affected area on
726 Rockall Bank lies a few kilometres inboard of this radius (Fig. 10). During that time (22 ka), the
727 ice sheet was still very close to its maximum extent, still occupying the Irish Shelf [Peters *et al.*,
728 2016], i.e. most of the ice load was still in place. Models based on relative sea-level data from
729 around Ireland and Scotland show that deglaciation was very rapid *after* 21 ka [Brooks *et al.*,
730 2008]. Therefore seismicity due to isostatic rebound as the cause of the 22 ka Rockall Bank slope
731 failure is unlikely. Therefore, we conclude that the generation of the 22 ka slope failure event

732 (slide C) was most probably unrelated to the climatic conditions. However, seismicity, unrelated
 733 to isostatic rebound, may have well been responsible for Slide C, even though the area is not
 734 generally very active seismically (Fig. 10)..



735

736 **Figure 10.** Location of study area (black box) relative to the extent of the area affected by
 737 isostatic downwarping (red dashed line) according to Lambeck (1996). Also shown are
 738 earthquake magnitudes since 1980 (from the Irish National Seismic Network).
 739

740 Seismicity due to isostatic rebound may have been responsible for Slide D and for the more
 741 recent event. The initiation area for Slide D is also within the area of influence of the main
 742 sweeping bottom current in the area that is strong enough to incise a moat at the base of slope of
 743 Rockall Bank.

744 Slide C was modelled by *Salmanidou et al.* [2017] and it was shown to have generated a 5-10m
 745 high tsunami that traversed Rockall Trough and impacted on the Co. Mayo coast, NW Ireland.
 746 However, given the timing, it is unlikely it reached the coast, having encountered the BIIS first,
 747 which at 22 ka was still occupying the Irish shelf [*Clark et al.*, 2012; *Peters et al.*, 2016;

748 *Sacchetti et al., 2012a*]. The ice shelf would likely have dampened the effect of the tsunami
749 wave. Although the question of whether or not slides C or D could have generated tsunamis is
750 beyond the scope of the present project, it is a topic worthy of further study as the affected slope
751 has not been fully evacuated and potential incipient scarps can be seen on the seafloor [
752 *Georgiopolou et al., 2013*] and their figure 6), and at least one, albeit much smaller event has
753 taken place following Slides C and D.

754 For tsunami risk assessments it is imperative that studies like the current one are undertaken
755 prior to modelling, in order to separate and distinguish the different events that constitute a slide
756 complex, otherwise the risk may be overestimated or even underestimated. Very large events
757 (several 100s of km³) that would generate more destructive tsunamis tend to have large
758 recurrence intervals and therefore, while the hazard exists, the risk may be considered small.
759 However, smaller- and medium-scale landslides (10s to a few 100s of km³) will have shorter
760 recurrence intervals and therefore the risk increases. Other factors such as sedimentation rates
761 and slope replenishment should also be considered when assessing risk of future slide events.
762 This study has demonstrated that (a) it is more likely that large buried slide events comprise
763 multiple smaller stacked events, (b) slide-prone areas can fail repeatedly along the same scarps
764 or regions, so these areas are at risk of failing again in the future, and c) slide events originating
765 on the same slope, with the same sediment source may have very different flow behaviour
766 probably because each slide creates new conditions for the slope and the seafloor that gets
767 traversed by the following slide. Perhaps the later slides tap into different lithologies or even
768 remobilize earlier slide deposits, which, in combination with the changed topography and the
769 increased bed roughness, may have significant effects in determining the flow behaviour,

770 allowing younger slides to disaggregate more, complicating further forecasting future slide
771 behaviours and tsunami modelling.

772 **6 Conclusions**

773 Using a set of newly-acquired high-resolution seismic profiles and gravity cores from the
774 depositional area of the Rockall Bank Slide Complex we have been able to demonstrate that:

- 775 • The complex comprises at least three large-scale slides of 200, 125, and 400 km³ each,
776 slides A, B and C in order of occurrence from oldest to youngest.
- 777 • Slides A and B occupy the southernmost part of the complex, while Slide C extends
778 across the middle and northernmost parts. This suggests that different parts of the slope
779 were unstable, although the southern scarp appears to have been unstable on at least two
780 occasions.
- 781 • The most recent events, Slides C and D and the small local event, are dated at 22 ka, 10
782 ka, and within the last 1000 years respectively.
- 783 • Based on the three most recent events, the recurrence period for slope instability in
784 Rockall Bank is about 10 ka, although this is based on only three data points and should
785 be taken with caution.
- 786 • The repeated instability focused on this part of the Rockall bank slope over such a long
787 period of time suggests that slope instability conditions are persistent through time and
788 that may indicate that this slope is inherently unstable.
- 789 • The concurrence of slide C with the beginning of deglaciation of the BIIS appears to be
790 coincidental.
- 791 • Multiple events from the same source area can and do generate events with different
792 flow behaviours.

793

794 **7 Acknowledgments**

795 Bathymetric data used in this paper can be found on www.infomar.ie. New core raw data (core
796 descriptions and MSCL measurements) and all CE11011 seismic profiles are provided as
797 supplemental material. Other cores used are published in literature. This study has been
798 supported by the Irish National Development Plan Marine Research Sub-Programme. We wish
799 to express our gratitude to the Officers, Scientists and Crew of Celtic Explorer expeditions
800 CE11011 and CE14011 for all the help and good times. AG would like to acknowledge the
801 Griffith Geoscience Awards and the Geological Survey Ireland Short Call awards (Grant 2015-
802 sc-036). Seismic data collection was supported by the Deutsche Forschungsgemeinschaft (Grant
803 KR2222/14-1). We are grateful to the reviewers Drs Alexandre Normandeau, Maureen Walton
804 and Alexey Portnov for their constructive comments.

805 **References**

806

- 807 Brooks, A. J., S. L. Bradley, R. L. Edwards, G. A. Milne, B. Horton, and I. Shennan (2008), Postglacial relative sea-
808 level observations from Ireland and their role in glacial rebound modelling, *Journal of Quaternary Science*, *23*(2),
809 175-192.
- 810 Bull, S., J. Cartwright, and M. Huuse (2009), A review of kinematic indicators from mass-transport complexes using
811 3D seismic data, *Marine and Petroleum Geology*, *26*(7), 1132-1151.
- 812 Carter, G. D. O., V. A. I. Huvenne, J. A. Gales, C. Lo Iacono, L. Marsh, A. Ougier-Simonin, K. Robert, and R. B.
813 Wynn (2018), Ongoing evolution of submarine canyon rockwalls; examples from the Whittard Canyon, Celtic
814 Margin (NE Atlantic), *Progress in Oceanography*.
- 815 Clark, C. D., A. L. C. Hughes, S. L. Greenwood, C. Jordan, and H. P. Sejrup (2012), Pattern and timing of retreat of
816 the last British-Irish Ice Sheet, *Quaternary Science Reviews*, *44*(0), 112-146.
- 817 Elliott, G. M., P. M. Shannon, P. D. W. Haughton, and L. K. Øvrebø (2010), The Rockall Bank Mass Flow:
818 Collapse of a moated contourite drift onlapping the eastern flank of Rockall Bank, west of Ireland, *Marine and*
819 *Petroleum Geology*, *27*(1), 92-107.
- 820 Faugères, J. C., E. Gonthier, F. Grousset, and J. Poutiers (1981), The Feni Drift: The importance and meaning of
821 slump deposits on the Eastern slope of the Rockall Bank, *Marine Geology*, *40*, M49-M57.
- 822 Faugères, J. C., D. A. V. Stow, P. Imbert, and A. Viana (1999), Seismic features diagnostic of contourite drifts,
823 *Marine Geology*, *162*(1), 1-38.
- 824 Flood, R. D., C. D. Hollister, and P. Lonsdale (1979), Disruption of the Feni sediment drift by debris flows from
825 Rockall Bank, *Marine Geology*, *32*(3-4), 311-334.
- 826 Frey Martinez, J., J. Cartwright, and B. Hall (2005), 3D seismic interpretation of slump complexes: examples from
827 the continental margin of Israel, *Basin Research*, *17*(1), 83-108.

- 828 Georgiopoulou, A., S. Benetti, S. M. Jones, and D. Wall (2010), RV Celtic Explorer CE10008, 3rd - 17th June, 2010
829 (Galway-Galway): Glacial and non-glacial sediment transport and seismic oceanography in the Rockall Trough, NE
830 Atlantic, *Rep.*, 24 pp, Marine Institute, Galway.
- 831 Georgiopoulou, A., S. Benetti, P. M. Shannon, P. D. W. Haughton, and S. McCarron (2012), Gravity flow deposits
832 in the deep Rockall Trough, Northeast Atlantic, in *Submarine mass movements and their consequences, Advances in
833 Natural and Technological Hazards Research*, edited by Y. Yamada, K. Kawamura, K. Ikehara, Y. Ogawa, R.
834 Urgeles, D. C. Mosher, J. D. Chaytor and M. Strasser, pp. 695-707, Springer, Dordrecht Heidelberg London New
835 York.
- 836 Georgiopoulou, A., P. M. Shannon, F. Sacchetti, P. D. W. Haughton, and S. Benetti (2013), Basement-controlled
837 multiple slope collapses, Rockall Bank Slide Complex, NE Atlantic, *Marine Geology*.
- 838 Hamilton, E. L., and R. T. Bachman (1982), Sound velocity and related properties of marine sediments, *The Journal
839 of the Acoustical Society of America*, 72(6), 1891.
- 840 Harkness, D. (1983), The extent of the natural ^{14}C deficiency in the coastal environment of the United Kingdom,
841 *Proceedings of the First International Symposium ^{14}C and Archaeology, PACT 8*, 351-364.
- 842 Holmes, R., D. Long, and L. R. Dodd (1998), Large-scale debrites and submarine landslides on the Barra Fan, west
843 of Britain, *Geological Society, London, Special Publications*, 129(1), 67-79.
- 844 Howe, J. A. (1996), Turbidite and contourite sediment waves in the northern Rockall trough, north Atlantic Ocean,
845 *Sedimentology*, 43(2), 219-234.
- 846 Hunt, J. E., R. B. Wynn, D. G. Masson, P. J. Talling, and D. A. H. Teagle (2011), Sedimentological and
847 geochemical evidence for multistage failure of volcanic island landslides: A case study from Icod landslide on north
848 Tenerife, Canary Islands, *Geochemistry, Geophysics, Geosystems*, 12(12), Q12007.
- 849 Johannessen, E. P., and R. J. Steel (2005), Shelf-margin clinoforms and prediction of deepwater sands, *Basin
850 Research*, 17, 521-550.
- 851 Jutzeler, M., J. D. L. White, P. J. Talling, M. McCanta, S. Morgan, A. Le Friant, and O. Ishizuka (2014), Coring
852 disturbances in IODP piston cores with implications for offshore record of volcanic events and the Missoula
853 megafloods, *Geochemistry, Geophysics, Geosystems*, 15(9), 3572-3590.
- 854 Lambeck, K. (1996), Glaciation and sea-level change for Ireland and the Irish Sea since Late Devensian/Midlandian
855 time, *Journal of the Geological Society, London*, 153, 853-872.
- 856 O'Reilly, B. M., P. W. Readman, and P. M. Shannon (2005), Slope failure, mass flow and bottom current processes
857 in the Rockall Trough, offshore Ireland, revealed by deep-tow sidescan sonar, *First break*, 23, 45-50.
- 858 O'Reilly, B. M., P. M. Shannon, and P. W. Readman (2007), Shelf to slope sedimentation processes and the impact
859 of Plio-Pleistocene glaciations in the northeast Atlantic, west of Ireland, *Marine Geology*, 238(1-4), 21-44.
- 860 Øvrebø, L. K., P. D. W. Haughton, and P. M. Shannon (2005), Temporal and spatial variations in late Quaternary
861 slope sedimentation along the undersupplied margins of the Rockall Trough, offshore west Ireland, *Norwegian
862 Journal of Geology*, 85, 279-294.
- 863 Peters, J. L., S. Benetti, P. Dunlop, C. Ó Cofaigh, S. G. Moreton, A. J. Wheeler, and C. D. Clark (2016),
864 Sedimentology and chronology of the advance and retreat of the last British-Irish Ice Sheet on the continental shelf
865 west of Ireland, *Quaternary Science Reviews*, 140, 101-124.
- 866 Sacchetti, F., S. Benetti, R. Quinn, and C. Ó Cofaigh (2012a), Glacial and post-glacial sedimentary processes in the
867 Irish Rockall Trough from an integrated acoustic analysis of near-seabed sediments, *Geo-Marine Letters*, 33(1), 49-
868 66.
- 869 Sacchetti, F., S. Benetti, A. Georgiopoulou, P. Dunlop, and R. Quinn (2011), Geomorphology of the Irish Rockall
870 Trough, North Atlantic Ocean, mapped from multibeam bathymetric and backscatter data, *Journal of Maps*, 2011,
871 60-81.
- 872 Sacchetti, F., S. Benetti, A. Georgiopoulou, P. M. Shannon, B. M. O'Reilly, P. Dunlop, R. Quinn, and C. Ó Cofaigh
873 (2012b), Deep-water geomorphology of the glaciated Irish margin from high-resolution marine geophysical data,
874 *Marine Geology*, 291-294(1), 113-131.
- 875 Salmanidou, D. M., A. Georgiopoulou, S. Guillas, and F. Dias (2018), Rheological considerations for the modelling
876 of submarine sliding at Rockall Bank, NE Atlantic Ocean, *Physics of Fluids*, 30(3), 030705.
- 877 Stoker, M. S. (1998), Sediment-drift development on the continental margin off NW Britain, in *Geological
878 processes on continental margins: sedimentation, mass-wasting and stability*, edited by M. S. Stoker, D. Evans and
879 A. Cramp, pp. 229-254, Geological Society Special Publication, London.
- 880 Stoker, M. S., T. C. E. van Weering, and T. Svaerdborg (2001), A Mid- to Late Cenozoic tectonostratigraphic
881 framework for the Rockall Trough, in *The petroleum exploration of Ireland's offshore basins*, edited by P. M.
882 Shannon, P. D. W. Haughton and D. V. Corcoran, pp. 411-438, Geological Society Special Publication, London.

- 883 Stoker, M. S., M. C. Akhurst, J. A. Howe, and D. A. V. Stow (1998), Sediment drifts and contourites on the
884 continental margin off northwest Britain, *Sedimentary Geology*, 115(1-4), 33-51.
- 885 Stoker, M. S., D. Praeg, B. O. Hjelstuen, J. S. Laberg, T. Nielsen, and P. M. Shannon (2005), Neogene stratigraphy
886 and the sedimentary and oceanographic development of the NW European Atlantic margin, *Marine and Petroleum*
887 *Geology*, 22(9-10), 977-1005.
- 888 Sumner, E. J., P. J. Talling, L. A. Amy, R. B. Wynn, C. J. Stevenson, and M. Frenz (2012), Facies architecture of
889 individual basin-plain turbidites: Comparison with existing models and implications for flow processes,
890 *Sedimentology*, 59(6), 1850-1887.
- 891 Unnithan, V., P. M. Shannon, K. McGrane, P. W. Readman, A. W. B. Jacob, R. Keary, and N. H. Kenyon (2001),
892 Slope instability and sediment redistribution in the Rockall Trough: constraints from GLORIA, in *The petroleum*
893 *exploration of Ireland's offshore basins*, edited by P. M. Shannon, P. D. W. Haughton and D. V. Corcoran,
894 Geological Society Special Publication, London.
- 895 van Weering, T. C. E., and S. de Rijk (1991), Sedimentation and climate-induced sediments on Feni Ridge,
896 Northeast Atlantic Ocean, *Marine Geology*, 101(1-4), 49-69.
- 897 Ward, S. N., and S. Day (2001), Cumbre Vieja Volcano-Potential Collapse and tsunamis at La Palma, Canary
898 Islands., *Geophysical Research Letters*, 28, 3397-3400.
- 899 Weaver, P. P. E., R. B. Wynn, N. H. Kenyon, and J. Evans (2000), Continental margin sedimentation, with special
900 reference to the north-east Atlantic margin., *Sedimentology*, 47(Suppl. 1), 239-256.
- 901 Wynn, R. B., and D. A. V. Stow (2002), Classification and characterisation of deep-water sediment waves, *Marine*
902 *Geology*, 192(1-3), 7-22.

903